Morphometry of tidal meander cutoffs indicates similarity to fluvial morphodynamics

C. Gao[1,2], E.D. Lazarus[3], A. D'Alpaos[2], M. Ghinassi[2], A. Ielpi[4], G. Parker[5,6], A. Rinaldo[7,8], P. Gao[9], Y.P. Wang[1,10], D. Tognin[7], and A. Finotello[2,*]

[1] Ministry of Education Key Laboratory for Coast and Island Development, School of Geographic and Oceanographic Sciences, Nanjing University, Nanjing, China.

[2] Dept. of Geosciences, University of Padova, Padova, Italy.

[3] School of Geography & Environmental Science, University of Southampton, Southampton, UK.

[4] Department of Earth, Environmental and Geographic Sciences, University of British Columbia-Okanagan, Kelowna, BC, Canada.

[5] Department of Civil & Environmental Engineering, University of Illinois, Urbana, IL, USA

[6] Department of Geology, University of Illinois, Urbana, IL, USA

[7] Department of Civil, Environmental, and Architectural Engineering, University of Padova, Padova, Italy

[8] Laboratory of Ecohydrology, Ecole Polytechnique Federale Lausanne, Lausanne, Switzerland

[9] Department of Geography and the Environment, Syracuse University, Syracuse, NY, USA.

[10] State Key Laboratory of Estuarine and Coastal Research, School of Marine Sciences, East China Normal University, Shanghai, China

* Corresponding author: Alvise Finotello (alvise.finotello@unipd.it)

Key Points:

- Tidal meander cutoffs are far more common than typically thought and share remarkable morphometric similarities with fluvial counterparts.
- Similar mechanisms trigger cutoffs in both tidal and fluvial landscapes, with differences arising only during post-cutoff evolution.
- Tidal cutoffs seldom disconnect from parent channels and rarely form oxbows due to the high hydrological connectivity of tidal wetlands.

Abstract

Sinuous channels wandering through coastal wetlands have been thought to lack lateral-migration features like meander cutoffs and oxbows, spurring the broad interpretation that tidal and fluvial meanders differ morphodynamically. Motivated by recent work showing similarities in planform dynamics between tidal and fluvial meandering channels, we analyzed meander neck cutoffs from diverse tidal and fluvial environments worldwide, and show that tidal cutoffs are widespread. Their perceived paucity stems from pronounced channel density and hydrological connectivity in coastal wetlands, comparatively small size of most tidal channels, and typically dense vegetation cover. Although these factors do not efface tidal meander cutoffs, they collectively inhibit oxbow formation and make tidal cutoffs ephemeral features that can escape detection. We argue that similar morphodynamic processes drive cutoff formation in tidal and fluvial landscapes, with differences arising only during post-cutoff evolution. Such process similarity has important implications for understanding coastal wetland ecomorphodynamics and predicting their long-term evolution.

Plain Language Summary

The sinuous channels that wander through tidal coastal wetlands look like meandering rivers. However, features of alluvial floodplains that indicate active river meandering over time, such as oxbow lakes and meander cutoffs, are difficult to find in tidal settings. Their apparent absence has led researchers to infer that tidal and fluvial meanders evolve differently. We re-examined this inference by identifying, measuring, and compiling examples of meander cutoffs from a variety of tidal coastal wetlands and fluvial floodplains worldwide. Our analysis suggests that the shapes and geometric properties of tidal and fluvial cutoffs are indeed remarkably similar. This indicates that while tidal and fluvial environments differ in many ways, they nevertheless share the same physical mechanism affecting meander morphodynamical evolution. Differences between tidal and fluvial meanders do arise after a meander is cut off. We observe that tidal meanders remain preferentially connected to the parent channel, preventing the formation of crescent-shaped oxbow lakes and thus making tidal cutoffs more difficult to detect. Our results indicate a close similarity in meandering channel behavior across tidal and fluvial systems, which opens new opportunities for how researchers model tidal wetlands, with important implications for the effective conservation and restoration of these critical ecosystems.

1 Introduction

Sinuous meandering channels are common in fluvial and coastal landscapes (Leopold et al., 1964). Meandering channels migrate laterally through erosion and deposition of sediment along the outer and inner banks, respectively, of individual meander bends. As meanders evolve, channels frequently shortcut themselves through cutoffs and form oxbow lakes (hereinafter "oxbows"; Dunne & Aalto, 2013; Schwenk et al., 2015; Stølum, 1996). Cutoffs play a critical role in channel and floodplain evolution by reducing channel sinuosity, modifying rates of lateral migration, and affecting floodplain sedimentology, stratigraphy, and sediment residence times (Camporeale et al., 2005; Howard & Hemberger, 1991; Zinger et al., 2011). Oxbows are important not only from ecological perspectives (Dieras, 2013; Thomas et al., 2022), but also because they retain signatures of the flow characteristics that shaped them (Guo et al., 2019). Collectively, the dynamics of meander cutoffs, of which oxbows are one consequence, have broad implications for the flux, storage, and sequestration of soil organic carbon (Torres et al., 2017).

While meandering river floodplains feature visible evidence of meander migration such as scroll bars and oxbows (Constantine & Dunne, 2008; Dunne & Aalto, 2013; Hooke, 2013), channels in tidal coastal floodplains have been thought to lack meander cutoffs and, therefore, morphological evidence of active meandering (Gabet, 1998; Johnson, 1929) (Figure 1). The apparent tendency for sinuous tidal channels to be fixed in place – or at least the relative subtlety of their meandering dynamics – has been variously ascribed to ecomorphodynamics peculiar to coastal settings, where flow bidirectionality is paramount (Fagherazzi et al., 2004; Hughes, 2012; Solari et al., 2002). However, recent studies highlighted morphodynamic commonalities between fluvial and tidal meanders, with similar planform dynamics, width-adjusted migration rates, and morphodynamic regimes in high-amplitude bends (Finotello et al., 2018, 2022; Gao, Finotello, & Wang, 2022; Leuven et al., 2016, 2018). This motivated us to question the perceived paucity of tidal meander cutoffs, and to further demonstrate the parallels between tidal and fluvial meandering channels. Here, we analyzed the planform geometry of N_t =600 tidal meander cutoffs identified in high-resolution satellite images from settings around the world, characterized by different tidal regimes, vegetation cover, and geomorphological backgrounds. Direct comparisons with cutoffs in meandering rivers (N_f=158) highlight geometric similarities that – with supporting evidence from theoretical, numerical, and field studies – are shared by morphodynamic processes in both tidal and fluvial realms.

2 Materials and Methods

2.1 Data collection

We used high-resolution satellite images, freely available from Google Earth Pro, to detect instances of meander cutoffs undisturbed by anthropic activities. The selected cutoffs encompass a wide variety of geographical locations, including coastal areas and inland alluvial plains, as well as a diversity of climatic and geological regions. Consequently, the sampled cutoffs reflect a range of hydrological and tidal regimes, sediment grain sizes, vegetation types, and land cover (Figure 1a-g). Our full dataset includes over 1200 examples of tidal cutoffs. Of these 1200 examples, 600 tidal cutoffs with clearly discernable boundaries were manually digitized as polygons using Google Earth Pro. The remainder lacked sufficient detail to be digitized due to poor preservation, dense vegetation canopy, low image resolution, complex morphology resulting from multiple cutoffs, or combinations of these factors, and were categorized as “unanalyzed cases” (Gao & Finotello, 2023). Furthermore, we obtained an additional set of 158 fluvial cutoffs specifically

digitized for comparative analyses. These cutoffs were extracted from rivers located in various regions, including the Amazon Basin, the conterminous USA and Alaska, Russia, Canada, Kazakhstan, and New Zealand. The selection was made to ensure a diverse range of channel sizes, with river widths spanning approximately four orders of magnitude (Figure 2).

Tidal cutoffs were also further classified based on tidal regime (microtidal n=315; mesotidal n=249; macrotidal n=36), vegetation cover (mangroves n=118; salt marshes n=433; tidal flats n=49), and geomorphological setting (bays n=164; back-barrier lagoons n=219; open coasts n=105; estuaries n=112) (Figure S1 in Supporting Information). The mean tidal range (MTR) for each study site was determined by analyzing tidal gauge data from Dong (2020) and the National Oceanic and Atmospheric Administration (https://tidesandcurrents.noaa.gov/), and individual study cases were classified as macro-tidal ($MTR > 4$ m), meso-tidal ($2 < MTR < 4$ m), and microtidal ($MTR < 2$ m).

We focus only on 'neck' cutoffs, formed when a high-amplitude loop gets isolated by the pinching connection of two adjacent bends. In the tidal settings we examined, we found no examples of 'chute' cutoffs, which are formed when a river bend is shortcutted by a new channel cutting through meander point bars – and possibly observed in large, sand-bedded, multi-thread estuarine channels (Leuven et al., 2016).

2.2 Data analysis

To calculate their morphometric parameters, cutoff polygons were projected into appropriate UTM coordinates and converted to binary images. The channel centerline was computed based on a standard skeletonization procedure and then resampled using standard cubic spline-fit polylines. Cutoff endpoints were determined as the two branchpoints of the polygon skeleton (Figure 1l). To further characterize cutoff planform features, we computed the curvature $\mathcal{C}$ ([m^{-1}]) of the channel centerline as $\mathcal{C} = -d\theta/ds$, where θ is the angle between the tangent to the channel axis and an arbitrarily selected reference direction, $x(s)$ and $y(s)$ are the Cartesian coordinates of a given centerline point, and s is the intrinsic (i.e., along-channel) coordinate, assumed to be positive in the upstream (i.e., landward) direction. Because flow orientation within tidal meanders changes with tidal phases, we hereinafter assume a river-like reference system in which the terms 'upstream' and 'downstream' refer to landward and seaward directions, respectively.

After computing curvature, a Savitzky–Golay low-pass filter was applied to smooth noise in the original signal. Then, the apex of any individual cutoff was identified as the locus of maximum curvature (Figure 1l), and the cutoff asymmetry index was computed as $\mathcal{A} = (\ell_u - \ell_d)/(\ell_u + \ell_d)$ ([-]) where ℓ_u and ℓ_d are the distances between the cutoff apex and its upstream and downstream endpoints, respectively (Figure 1l). Negative values of $\mathcal{A}$ correspond to upstream-skewed cutoffs, and positive values of $\mathcal{A}$ to downstream-skewed cutoffs. Other morphometric parameters were also calculated, including: average channel width W ([-]); cutoff intrinsic length $\ell = \ell_u + \ell_d$ ([m]); cutoff cartesian length L ([m]), which is the planar distance between cutoff endpoints; cutoff sinuosity $\chi = \ell/L$ ([-]); cutoff amplitude A ([-]), computed as the maximum point-line distance between the cutoff centerline and the line connecting the two cutoff endpoints; cutoff radius of curvature R ([m]), defined as the radius of the best-fitting circle through all cutoff axis points; and flow-diversion angle Φ between the cutoff and its parent channel (Figure 1l). Because of bidirectional flow through tidal channels, morphodynamically meaningful flow-diversion angles can be identified at both the cutoff upstream (Φ_u) and downstream (Φ_d) ends. By comparison, because of the unidirectional flow through river channels, only the upstream flow-diversion angle (Φ_u) is morphodynamically meaningful for fluvial cutoffs (Dieras, 2013).

To directly compare meander cutoffs of different sizes, dimensional morphometric variables were normalized using channel width (W), such that width-adjusted cutoff radius of curvature, amplitude, and lengths are defined as $R^* = R/W$, $A^* = A/W$, $L^* = L/W$, and $\ell^* = \ell/W$.

3 Results

Dimensional morphometric features of individual cutoffs – R, A, and ℓ – all exhibit statistically significant (p-value < 0.01) power-law relationships to cutoff width W with matching best-fit power-law exponents and limited separation in power-law scaling constants (Figure 2 and Figure S2 in Supporting Information). We also found a statistically significant quasi-linear relation between L and W (Figure S3 in Supporting Information), with $L \cong W$. The latter has been described previously as the condition leading to neck cutoff (Li et al., 2022), whereas L<W represents a geometrically impossible configuration (Hayden et al., 2021). Similarly, radius of curvature R=$W/2$ represents a physically meaningful lower bound, since the edges of a channel centerline with a radius of curvature smaller than half its width would intersect each other (Hayden et al., 2021). Although theoretically there are no physical limits to the development of both A and ℓ (besides the basic requirements that A>0 and ℓ>L in order for a centerline to be sinuous), the prevalence of smaller curves weights the distribution of meander features toward the physically meaningful lower bound (Vermeulen et al., 2016). For these reasons, the scaling similarity in dimensional metrics reported in Figure 2 is likely due to the finite-width nature of the sinuous features we measured, rather than representing a suitable diagnostic with which to distinguish the fluvial or tidal nature of meander cutoffs. Indeed, previous studies suggest that dimensionless meander morphometrics should be used to infer morphological similarity (Frascati & Lanzoni, 2009; Howard & Hemberger, 1991). We thus performed Kolmogorov-Smirnov (KS) tests (α=0.05) on dimensionless morphometric descriptors to highlight that tidal cutoffs are typically less sinuous (i.e., lower χ) and feature smaller with-adjusted radii (R^*), amplitudes (A^*), and intrinsic lengths (ℓ^*) (Figure 3 and Table S1 in Supporting Information).

Since meander size and sinuosity are expected to increase with time, our findings could be broadly interpreted as tidal cutoffs being less morphodynamically mature (i.e., less sinuous and planimetrically complex) than their fluvial counterparts, thus pointing to a faster evolutionary trajectory from meander inception to cutoffs. However, similar width-adjusted meander migration rates in tidal and fluvial settings (Finotello et al., 2018) contrast with such an interpretation. Furthermore, KS tests demonstrate similar values of asymmetry ($\mathcal{A}$) and upstream flow-diversion angle (Φ_u) in tidal and fluvial cutoffs (Figure 3 and Table S1 in Supporting Information). Given that neither of these parameters are affected by meander size, the observed similarity not only reflects similar morphodynamic maturity but also suggest shared cutoff-triggering mechanisms, likely associated with the planform configuration of the parent channel (Dieras, 2013). Notably, both fluvial and tidal cutoffs exhibit negative median and peak values of the asymmetry index $\mathcal{A}$ (Figure 3e). That is, both types of cutoffs tend to be upstream-skewed, supporting similarity in their dominant morphodynamic regime (*sensu* Seminara et al., 2001). This observation likely stems from the morphodynamic dominance, in tidal channels, of either flood or (more commonly) ebb flows that effectively render tidal meanders similar to their fluvial counterparts featuring unidirectional flows (Fagherazzi et al., 2004; Kleinhans et al., 2009).

We thus suggest that the smaller size of tidal relative to fluvial cutoffs does not depend on fundamental differences in their morphodynamics, and is rather dictated by peculiar hydro-, eco-, and geo-morphological features of tidal wetlands. Specifically, we hypothesize that the dense distribution of tidal channels that typically characterizes tidal wetlands accounts for the reduced

size and sinuosity of tidal cutoffs, with enhanced hydrological connectivity explaining the apparent paucity of cutoff traces in tidal environments as we discuss below.

4 Discussion

4.1 Dense channel distribution limits stream meandering and cutoff formation

Meander migration in densely channeled tidal floodplains shapes the landscape differently than in fluvial contexts, where rivers can freely migrate laterally without intercepting other channels and confluences are comparatively infrequent. Tidal wetlands are characterized by high drainage density (taken, *sensu* Marani et al., 2003, as the mean shortest distance that a parcel of water place on the wetland surface would need to travel before reaching the closest channel) that limits meander dynamics by preventing channels from freely migrating and meanders from fully developing without intercepting adjoining streams (Letzsch & Frey, 1980; Vilas et al., 1999). A similar dynamic is described in multi-thread, anabranching rivers with individual sinuous anabranches, where enhanced channel density limits cutoff formation (Schumm et al., 1996). Accordingly, evidence from modern and ancient deposits shows that channel piracies (i.e., stream captures) in dense tidal networks (Figure S4 in Supporting Information) limit the lateral accretion of point bar bodies and can modify the network-scale distribution of the tidal prism, feeding back into the long term ecomorphodynamic evolution of the entire tidal system (Cosma et al., 2020; Finotello, Ghinassi, et al., 2020). Hence, enhanced channel density limits tidal meander dynamics and cutoff formation.

Our hypothesis is further corroborated by systematic statistically significant differences observed in the distributions of R^*, A^*, L^*, and χ as a function of vegetation cover, with effects of tidal regime and geomorphological background being significant but less systematic (Figure 3 and Tables S2 to S13 in Supporting Information). Tidal cutoffs in salt marshes are smaller and less sinuous than those found in mangrove forests and tidal flats (Figure 3). This finding aligns with observations of tidal channel networks being denser in vegetated settings, especially in salt marshes (Kearney & Fagherazzi, 2016; Schwarz et al., 2022), and corroborates the idea that meander cutoffs in densely channelized tidal wetlands cannot grow large and highly sinuous because lateral migration would often result in channel piracies. Similar cutoff asymmetries ($\mathcal{A}$) and flow-diversion angles (Φ_u, Φ_d) among distinct tidal settings also support similarity in the morphodynamic processes responsible for cutoff development. Kolmogorov-Smirnov tests reveal significant differences in distributions of Φ_u, Φ_d, and $\mathcal{A}$ only based on geomorphological setting (Tables S2 to S13 in Supporting Information), but we find no differences in these morphometrics as a function of tidal range and vegetation cover despite the potential influence that both controls can exert on channel bank erosion (Gao, Finotello, D'Alpaos, et al., 2022; Gasparotto et al., 2022; Zhao et al., 2022).

4.2 Hydrological connectivity control on post-cutoff development

To further substantiate that differences in tidal and fluvial cutoff morphology do not stem from dissimilarities in meander morphodynamics, we also examined the connection state of individual cutoffs with their parent channels. Once a river meander is cut off, a plug bar forms in response to flow separation and reduced energy conditions, leading to the rapid deposition of coarse sediment and blockage of both cutoff entrances (Toonen et al., 2012). Eventually, the cutoff becomes completely disconnected from the parent channel and forms an oxbow. Based on the presence and position of plug bars in our tidal and fluvial examples, we classified cutoffs into four groups:

completely connected, upstream connected, downstream connected, and disconnected (Figure 4). The upstream- and downstream-connected cases can also be merged into a broader category of partially connected cutoffs. Whereas more than 43% of fluvial cutoffs in our dataset are entirely disconnected and only 28% are completely connected (Figure 4a), tidal cutoffs tend to remain connected to their parent channels, with 87% of examples completely connected, 9% partially connected, and only 4% entirely disconnected (Figure 4a).

This difference in the connection state of tidal versus fluvial cutoffs is apparently not a function of tidal range, vegetation cover, and geomorphological setting (Figure 4), effectively ruling out the possibility that the observed lack of plug bars in tidal cutoffs depends on site-specific landscape features (e.g., sediment grain size; Kleinhans et al., 2024) Moreover, similar flow-diversion angles are observed in all our study cases, with median values consistently ranging between 105° and 108° (Figure 4b,c) and further pointing to similar cutoff-triggering mechanisms in fluvial and tidal landscapes. Morphological differences thus can be expected to emerge once cutoffs have formed. The percentage of completely connected fluvial cutoffs decreases as the flow-diversion angle increases, implying that larger Φ_u promote the formation of plug bars and oxbows (Figure 4d). In contrast, tidal cutoffs tend to remain connected to their parent channel irrespective of flow-diversion angles, whether upstream or downstream (Figure 4d and Figure S5 in Supporting Information).

Therefore, unlike fluvial analogs, most tidal cutoffs remain hydrodynamically active to some extent: periodic overbank flows in tidal channels result in significant rates of lateral flow injections from the adjoining tidal floodplains during ebb tide, which maintain active flows even in cutoff bends and prevent plug-bar formation by keeping the cutoff entrance flushed. Notably, some tidal cutoffs may also remain connected to other active parts of the network through minor lateral tributaries flowing directly into the cutoff (Figure 1a-i and Figure S6 in Supporting Information). Hence, pronounced hydrological connectivity in tidal wetlands prevents the formation of plug bars and the subsequent evolution of tidal cutoffs into oxbows. Such an evolutionary trajectory clearly differs from fluvial cutoffs, which are typically abandoned and receive water and sediment input almost exclusively during major floods either through minor tie channels carved through the plug bar (Rowland et al., 2009) or as the entire alluvial plain floods (Shen et al., 2021).

Among the partially connected cutoffs in our dataset, the fluvial ones are preferentially connected with their parent channels at the upstream end: plug bars tend to form at the cutoff downstream end where flow separations and recirculation create a zone of dead velocity that hinders mixing and promotes sediment deposition (e.g., Turnipseed et al., 2021). In contrast, the few partially connected tidal cutoffs on record, tend to maintain connectivity at the downstream end (Figure 4a), aligned with the direction of typically dominant ebb flows that seemingly keep the cutoff downstream end periodically flushed.

4.3 Meander cutoffs in tidal coastal landscapes: rare or everywhere?

Abundant tidal cutoffs akin to oxbow-rich alluvial floodplains can be found in some tidal settings with possibly lower drainage density and/or sediment supply that limits cutoff infill and vegetation encroachment (Figure 1f-i; Figures S7, S8 in Supporting Information). This further corroborates the observation that tidal and fluvial meandering channels not only evolve through similar morphodynamic processes, but also that tidal meanders are as prone to form cutoffs as their fluvial counterparts given conducive environmental conditions. Given the apparent ubiquity of cutoffs across a variety of tidal environments, why has the notion that sinuous tidal channel bends are inherently unlikely to cut off prevailed so long (Gabet, 1998; Johnson, 1929)?

We suggest that, first, the characteristic width and amplitude of fluvial cutoffs may not vary significantly along a given reach of a meandering river between major tributaries, whereas meander cutoffs within a given tidal wetland can occur across a broad range of meander wavelengths and widths (Finotello, D'Alpaos, et al., 2020). Low-order, narrow tidal creeks are more frequently found than higher-order, wide channels and are thus the most likely to express cutoff development (Figure 1a-i; Figures S7, S8 in Supporting Information). Yet small channels produce small cutoffs, which are especially challenging to observe from a broader spatial vantage, particularly when the vegetation canopy is dense (e.g., in mangrove forests, Figure S9 in Supporting Information).

Another consideration is the sustained rate of vertical accretion that characterizes tidal wetlands, coupled with halophytic vegetation that can tolerate significant waterlogging stress. These factors may becloud cutoff traces (Figure 1b,d,f-i and Figure S9 in Supporting Information) through rapid sedimentation in the less hydrodynamically active portions of the cutoff, and the subsequent encroachment of vegetation. This levels out cutoff geomorphic expressions and further hinders their identification from aerial images. Although similar reasoning could apply to fluvial floodplains, reduced overbank sediment supply and slower rates of riparian vegetation growth in permanently waterlogged areas may prolong the timescale required to fill oxbows, making large river-cutoff scars identifiable from aerial photos for much longer periods (Kleinhans et al., 2024) (Figure 1j,k).

The apparent absence of tidal cutoffs is thus more an artifact of observations than a consequence of physical mechanisms. High drainage densities in tidal wetlands surely constrain the freely meandering of tidal channels (Figure S10 in Supporting Information). Yet the relatively small size of most tidal channels, along with the distinctive hydrological characteristics of tidal wetlands, contribute to the transient nature of tidal cutoffs and make them challenging to record. That is, unlike other features of meandering channels that might jump out at the observer, to find tidal cutoffs one has to go carefully looking for them.

The implied morphodynamic similarity between tidal and fluvial meanders is by no means diminished by the absence of prominent scroll bars in tidal wetlands, standing in stark contrast to river floodplains that often – but not always (Candel et al., 2020, 2021) – showcase intricate arrangements of sub-parallel scrolls indicative of previous channel locations (Figure 1k) (Strick et al., 2018). While there is no consensus on what drives the formation of scroll bars (van de Lageweg et al., 2014), we offer two possible, not mutually exclusive explanations for the absence of scroll bars in tidal meanders. One possibility is that tidal meanders undergo small and yet continuous incremental migrations, unlike fluvial meanders that tend to migrate more episodically during major flood events (Mason & Mohrig, 2019; Wu et al., 2016). Another hypothesis is that sustained rates of vertical aggradation relative to lateral channel migration in tidal wetlands prevent scroll bars by systematically overshadowing any topographic irregularities (Brivio et al., 2016; Cosma et al., 2019). This explanation aligns with the lack of scroll bars in meandering streamflows evolving through curvature-driven fluvial-like mechanisms in aggradational settings such as coastal backwater areas (Swartz et al., 2020), peatlands (Candel et al., 2017), and submarine turbidity-current channels (Jobe et al., 2016; Morris et al., 2024).

5 Implications and Conclusions

Our findings demonstrate that meandering channels in tidal wetlands are as capable of forming meander cutoffs as their fluvial counterparts. From the morphometric evidence we have compiled, we suggest that the morphodynamic processes that drive tidal and fluvial cutoff development are

fundamentally similar, with substantial differences arising only after cutoffs have formed. Rather than forming oxbows, tidal cutoffs remain preferentially connected to their parent channel owing to the pronounced hydrological connectivity that characterizes tidal wetlands. Tidal meander cutoffs thus continue to drain (and help flood) the surrounding wetlands, remaining active and integral parts of the overall tidal channel network. Considered alongside previous theoretical, numerical, and field observations (Finotello et al., 2018, 2022; Gao, Finotello, & Wang, 2022; Leuven et al., 2018), our results indicate a complete morphodynamic analogy between tidal and fluvial meandering channels from meander inception to cutoff. Unified tidal and fluvial meander morphodynamics enable extension of classical techniques for modeling meandering rivers (Bogoni et al., 2017; Howard & Knutson, 1984; Parker et al., 2011; Seminara et al., 2001) to ecomorphodynamic models of tidal wetlands, where meandering is ubiquitous and yet routinely omitted. Such an advance in numerical modeling would have important implications for the conservation and restoration of critically endangered tidal wetlands – for example, by helping improve assessments and estimations of past, present, and future blue carbon fluxes.

Acknowledgments

We are grateful for constructive reviews from M. Kleinhans and one anonymous reviewer, as well as for recommendations from the Editorial Office, which improved this manuscript.

This study is funded by the European Union – NextGenerationEU and by the University of Padua under the 2021 STARS Grants@Unipd programme "TiDyLLy- Tidal networks dynamics as drivers for ecomorphodynamics of low-lying coastal area" (to AF), as well as by a China Scholarship Council (CSC) scholarships (202106190084, to CG). AI is supported by a Discovery Grant from the Natural Sciences and Engineering Research Council of Canada. AF, MG, and ADA also acknowledge support by the Italian Ministry of University and Research (MUR) through the project titled 'The Geosciences for Sustainable Development' (Budget MUR - Dipartimenti di Eccellenza 2023-2027; Project ID C93C23002690001)

Conflict of Interest Statement

The authors declare no conflict of interest.

Open Research

All the data presented and analyzed in this paper are freely available from a public Zenodo folder (Gao & Finotello, 2023)

References

Bogoni, M., Putti, M., & Lanzoni, S. (2017). Modeling meander morphodynamics over self-formed heterogeneous floodplains. *Water Resources Research*, *53*(6), 5137–5157. https://doi.org/10.1002/2017WR020726

Brivio, L., Ghinassi, M., D'Alpaos, A., Finotello, A., Fontana, A., Roner, M., & Howes, N. (2016). Aggradation and lateral migration shaping geometry of a tidal point bar: An example from salt marshes of the Northern Venice Lagoon (Italy). *Sedimentary Geology*, *343*, 141–155. https://doi.org/10.1016/j.sedgeo.2016.08.005

Camporeale, C., Perona, P., Porporato, A., & Ridolfi, L. (2005). On the long-term behavior of meandering rivers. *Water Resources Research*, *41*(12), 1–13. https://doi.org/10.1029/2005WR004109

Candel, J. H. J., Makaske, B., Storms, J. E. A., & Wallinga, J. (2017). Oblique aggradation: a novel explanation for sinuosity of low-energy streams in peat-filled valley systems. *Earth Surface*

Processes and Landforms, *42*(15), 2679–2696. https://doi.org/10.1002/esp.4100
Candel, J. H. J., Makaske, B., Kijm, N., Kleinhans, M. G., Storms, J. E. A., & Wallinga, J. (2020). Self-constraining of low-energy rivers explains low channel mobility and tortuous planforms. *Depositional Record*, *6*(3), 648–669. https://doi.org/10.1002/dep2.112
Candel, J. H. J., Kleinhans, M. G., Makaske, B., & Wallinga, J. (2021). Predicting river channel pattern based on stream power, bed material and bank strength. *Progress in Physical Geography*, *45*(2), 253–278. https://doi.org/10.1177/0309133320948831
Constantine, J. A., & Dunne, T. (2008). Meander cutoff and the controls on the production of oxbow lakes. *Geology*, *36*(1), 23–26. https://doi.org/10.1130/G24130A.1
Cosma, M., Ghinassi, M., D'Alpaos, A., Roner, M., Finotello, A., Tommasini, L., & Gatto, R. (2019). Point-bar brink and channel thalweg trajectories depicting interaction between vertical and lateral shifts of microtidal channels in the Venice Lagoon (Italy). *Geomorphology*, *342*, 37–50. https://doi.org/10.1016/j.geomorph.2019.06.009
Cosma, M., Finotello, A., Ielpi, A., Ventra, D., Oms, O., D'Alpaos, A., & Ghinassi, M. (2020). Piracy-controlled geometry of tide-dominated point bars: Combined evidence from ancient sedimentary successions and modern channel networks. *Geomorphology*, *370*, 107402. https://doi.org/10.1016/j.geomorph.2020.107402
Dieras, P. L. (2013). The Persistence of Oxbow Lakes as Aquatic Habitats : an Assessment of Rates of Change and Patterns of Alluviation Doctorate of Philosophy, 177. Retrieved from http://orca.cf.ac.uk/49392/
Dunne, T., & Aalto, R. E. (2013). Large River Floodplains. In J. E. Schroder & E. Wohl (Eds.), *Treatise on Geomorphology* (Vol. 9, pp. 645–678). Elsevier. https://doi.org/10.1016/B978-0-12-374739-6.00258-X
Fagherazzi, S., Gabet, E. J., & Furbish, D. J. (2004). The effect of bidirectional flow on tidal channel planforms. *Earth Surface Processes and Landforms*, *29*(3), 295–309. https://doi.org/10.1002/esp.1016
Finotello, A., Lanzoni, S., Ghinassi, M., Marani, M., Rinaldo, A., & D'Alpaos, A. (2018). Field migration rates of tidal meanders recapitulate fluvial morphodynamics. *Proceedings of the National Academy of Sciences*, *115*(7), 1463–1468. https://doi.org/10.1073/pnas.1711330115
Finotello, A., D'Alpaos, A., Bogoni, M., Ghinassi, M., & Lanzoni, S. (2020). Remotely-sensed planform morphologies reveal fluvial and tidal nature of meandering channels. *Scientific Reports*, *10*(1), 1–13. https://doi.org/10.1038/s41598-019-56992-w
Finotello, A., Ghinassi, M., Carniello, L., Belluco, E., Pivato, M., Tommasini, L., & D'Alpaos, A. (2020). Three-Dimensional Flow Structures and Morphodynamic Evolution of Microtidal Meandering Channels. *Water Resources Research*, *56*(7), e2020WR027822. https://doi.org/10.1029/2020WR027822
Finotello, A., Capperucci, R. M., Bartholomä, A., D'Alpaos, A., & Ghinassi, M. (2022). Morpho-sedimentary evolution of a microtidal meandering channel driven by 130 years of natural and anthropogenic modifications of the Venice Lagoon (Italy). *Earth Surface Processes and Landforms*, *47*(10), 2580–2596. https://doi.org/10.1002/esp.5396
Frascati, A., & Lanzoni, S. (2009). Morphodynamic regime and long-term evolution of meandering rivers. *Journal of Geophysical Research: Earth Surface*, *114*(2), 1–12. https://doi.org/10.1029/2008JF001101
Gabet, E. J. (1998). Lateral Migration and Bank Erosion in a Saltmarsh Tidal Channel in San Francisco Bay, California. *Estuaries*, *21*(4), 745. https://doi.org/10.2307/1353278
Gao, C., & Finotello, A. (2023). Morphometry of widespread tidal meander cutoffs discloses

similarity to fluvial morphodynamics. [Dataset]. https://doi.org/10.5281/zenodo.8229300
Gao, C., Finotello, A., D'Alpaos, A., Ghinassi, M., Carniello, L., Pan, Y., et al. (2022). Hydrodynamics of Meander Bends in Intertidal Mudflats: A Field Study From the Macrotidal Yangkou Coast, China. *Water Resources Research*, *58*(12), 1–28. https://doi.org/10.1029/2022WR033234
Gao, C., Finotello, A., & Wang, Y. P. (2022). Predominant landward skewing of tidal meanders. *Earth Surface Processes and Landforms*, (July), 1–17. https://doi.org/10.1002/esp.5452
Gasparotto, A., Darby, S. E., Leyland, J., & Carling, P. A. (2022). Water level fluctuations drive bank instability in a hypertidal estuary. *Earth Surface Dynamics*, *2080*(September), 1–28.
Guo, X., Chen, D., & Parker, G. (2019). Flow directionality of pristine meandering rivers is embedded in the skewing of high-amplitude bends and neck cutoffs. *Proceedings of the National Academy of Sciences of the United States of America*, *116*(47), 23448–23454. https://doi.org/10.1073/pnas.1910874116
Hayden, A. T., Lamb, M. P., & Carney, A. J. (2021). Similar curvature-to-width ratios for channels and channel belts: Implications for paleo-hydraulics of fluvial ridges on Mars. *Geology*, *49*(7), 837–841. https://doi.org/10.1130/G48370.1
Hooke, J. M. (2013). River Meandering. In E. Wohl & Schroder (Eds.), *Treatise on Geomorphology* (Vol. 9, pp. 260–288). Washington: Elsevier. https://doi.org/10.1016/B978-0-12-374739-6.00241-4
Howard, A. D., & Hemberger, A. T. (1991). Multivariate characterization of meandering. *Geomorphology*, *4*(3–4), 161–186. https://doi.org/10.1016/0169-555X(91)90002-R
Howard, A. D., & Knutson, T. R. (1984). Sufficient conditions for river meandering: A simulation approach. *Water Resources Research*, *20*(11), 1659–1667. https://doi.org/10.1029/WR020i011p01659
Hughes, Z. J. (2012). Tidal channels on tidal flats and marshes. In R. A. Davis & R. W. Dalrymple (Eds.), *Principles of Tidal Sedimentology* (Springer, pp. 269–300). Dordrecht: Springer. https://doi.org/10.1007/978-94-007-0123-6_11
Jobe, Z. R., Howes, N. C., & Auchter, N. C. (2016). Comparing submarine and fluvial channel kinematics: Implications for stratigraphic architecture. *Geology*, *44*(11), 931–934. https://doi.org/10.1130/G38158.1
Johnson, D. (1929). Meanders in Tidal Streams: A Review and Discussion. *Geographical Review*, *19*(1), 135. https://doi.org/10.2307/208081
Kearney, W. S., & Fagherazzi, S. (2016). Salt marsh vegetation promotes efficient tidal channel networks. *Nature Communications*, *7*, 1–7. https://doi.org/10.1038/ncomms12287
Kleinhans, M. G., Schuurman, F., Bakx, W., & Markies, H. (2009). Meandering channel dynamics in highly cohesive sediment on an intertidal mud flat in the Westerschelde estuary, the Netherlands. *Geomorphology*, *105*(3–4), 261–276. https://doi.org/10.1016/j.geomorph.2008.10.005
Kleinhans, M. G., McMahon, W. J., & Davies, N. S. (2024). What even is a meandering river? A philosophy-enhanced synthesis of multilevel causes and systemic interactions contributing to river meandering. *Geological Society, London, Special Publications*, *540*(1). https://doi.org/10.1144/sp540-2022-138
van de Lageweg, W. I., van Dijk, W. M., Baar, A. W., Rutten, J., & Kleinhans, M. G. (2014). Bank pull or bar push: What drives scroll-bar formation in meandering rivers? *Geology*, *42*(4), 319–322. https://doi.org/10.1130/G35192.1
Leopold, L. B., Wolman, M. G., & Miller, J. P. (1964). *Fluvial processes in geomorphology*

(Freeman). San Francisco. Retrieved from http://catalogue.nla.gov.au/Record/2338901
Letzsch, W. S., & Frey, R. W. (1980). Deposition and erosion in a Holocene salt marsh, Sapelo Island, Georgia. *Journal of Sedimentary Petrology*, *50*(2), 529–542. https://doi.org/10.1306/212F7A45-2B24-11D7-8648000102C1865D
Leuven, J. R. F. W., Kleinhans, M. G., Weisscher, S. A. H., & van der Vegt, M. (2016). Tidal sand bar dimensions and shapes in estuaries. *Earth-Science Reviews*, *161*, 204–223. https://doi.org/10.1016/j.earscirev.2016.08.004
Leuven, J. R. F. W., van Maanen, B., Lexmond, B. R., van der Hoek, B. V., Spruijt, M. J., & Kleinhans, M. G. (2018). Dimensions of fluvial-tidal meanders: Are they disproportionally large? *Geology*, *46*(10), 923–926. https://doi.org/10.1130/G45144.1
Li, Z., Gao, P., You, Y., Finotello, A., & Ielpi, A. (2022). Delayed neck cutoff in the meandering Black River of the Qinghai–Tibet plateau. *Earth Surface Processes and Landforms*, (September 2022), 1–12. https://doi.org/10.1002/esp.5534
Marani, M., Belluco, E., D'Alpaos, A., Defina, A., Lanzoni, S., & Rinaldo, A. (2003). On the drainage density of tidal networks. *Water Resources Research*, *39*(2), 1–11. https://doi.org/10.1029/2001WR001051
Mason, J., & Mohrig, D. (2019). Scroll bars are inner bank levees along meandering river bends. *Earth Surface Processes and Landforms*, *44*(13), 2649–2659. https://doi.org/10.1002/esp.4690
Morris, P. D., Sylvester, Z., Covault, J. A., Mohrig, D., & Dunlap, D. (2024). Fluvial-style migration controls autogenic aggradation in submarine channels: Joshua Channel, eastern Gulf of Mexico. In A. Finotello, Z. Sylvester, & P. R. Durkin (Eds.), *Meandering Streamflows: Patterns and Processes across Landscapes and Scales* (Vol. 540). Geological Society, London, Special Publications. https://doi.org/10.1144/SP540-2022-123
Parker, G., Shimizu, Y., Wilkerson, G. V., Eke, E. C., Abad, J. D., Lauer, J. W., et al. (2011). A new framework for modeling the migration of meandering rivers. *Earth Surface Processes and Landforms*, *36*(1), 70–86. https://doi.org/10.1002/esp.2113
Rowland, J. C., Dietrich, W. E., Day, G., & Parker, G. (2009). Formation and maintenance of single-thread tie channels entering floodplain lakes: Observations from three diverse river systems. *Journal of Geophysical Research: Earth Surface*, *114*(2), 1–19. https://doi.org/10.1029/2008JF001073
Schumm, S. A., Erskine, W. D., & Tilleard, J. W. (1996). Morphology, hydrology, and evolution of the anastomosing Ovens and King Rivers, Victoria, Australia. *Bulletin of the Geological Society of America*, *108*(10), 1212–1224. https://doi.org/10.1130/0016-7606(1996)108<1212:MHAEOT>2.3.CO;2
Schwarz, C., van Rees, F., Xie, D., Kleinhans, M. G., & van Maanen, B. (2022). Salt marshes create more extensive channel networks than mangroves. *Nature Communications*, *13*(1), 1–9. https://doi.org/10.1038/s41467-022-29654-1
Schwenk, J., Lanzoni, S., & Foufoula-Georgiou, E. (2015). The life of a meander bend: Connecting shape and dynamics via analysis of a numerical model. *Journal of Geophysical Research: Earth Surface*, *120*(4), 690–710. https://doi.org/10.1002/2014JF003252
Seminara, G., Zolezzi, G., Tubino, M., & Zardi, D. (2001). Downstream and upstream influence in river meandering. Part 2. Planimetric development. *Journal of Fluid Mechanics*, *438*, 213–230. https://doi.org/10.1017/S0022112001004281
Shen, Z., Aeschliman, M., & Conway, N. (2021). Paleodischarge reconstruction using oxbow lake sediments complicated by shifting hydrological connectivity. *Quaternary International*,

604(July), 75–81. https://doi.org/10.1016/j.quaint.2021.07.004
Solari, L., Seminara, G., Lanzoni, S., Marani, M., & Rinaldo, A. (2002). Sand bars in tidal channels part 2. Tidal meanders. *Journal of Fluid Mechanics*, *451*(January), 203–238. https://doi.org/10.1017/s0022112001006565
Stølum, H. H. (1996). River meandering as a self-organization process. *Science*, *271*(5256), 1710–1713. https://doi.org/10.1126/science.271.5256.1710
Strick, R. J. P., Ashworth, P. J., Awcock, G., & Lewin, J. (2018). Morphology and spacing of river meander scrolls. *Geomorphology*, *310*, 57–68. https://doi.org/10.1016/j.geomorph.2018.03.005
Swartz, J. M., Goudge, T. A., & Mohrig, D. C. (2020). Quantifying Coastal Fluvial Morphodynamics Over the Last 100 Years on the Lower Rio Grande, USA and Mexico. *Journal of Geophysical Research: Earth Surface*, *125*(6), 1–16. https://doi.org/10.1029/2019JF005443
Thomas, S. S., Constantine, J. A., Dethier, D., Thoman, J. W., Racela, J., Blau, E., & Landis, J. D. (2022). The importance of oxbow lakes in the floodplain storage of pollutants. *Geology*, *50*(4), 392–396. https://doi.org/10.1130/G49427.1
Toonen, W. H. J., Kleinhans, M. G., & Cohen, K. M. (2012). Sedimentary architecture of abandoned channel fills. *Earth Surface Processes and Landforms*, *37*(4), 459–472. https://doi.org/10.1002/esp.3189
Torres, M. A., Limaye, A. B., Ganti, V., Lamb, M. P., Joshua West, A., & Fischer, W. W. (2017). Model predictions of long-lived storage of organic carbon in river deposits. *Earth Surface Dynamics*, *5*(4), 711–730. https://doi.org/10.5194/esurf-5-711-2017
Turnipseed, C., Konsoer, K., Richards, D., & Willson, C. (2021). Numerical Modeling of Two-Dimensional Hydrodynamics in a Highly Curving and Actively Evolving Neck Cutoff Under Different Hydrologic Conditions. *Water Resources Research*, *57*(2), 1–14. https://doi.org/10.1029/2020WR027329
Vermeulen, B., Hoitink, A. J. F., Zolezzi, G., Abad, J. D., & Aalto, R. (2016). Multiscale structure of meanders. *Geophysical Research Letters*, *43*(7), 3288–3297. https://doi.org/10.1002/2016GL068238
Vilas, F., Arche, A., Ferrero, M., & Isla, F. (1999). Subantarctic macrotidal flats, cheniers and beaches in San Sebastian Bay, Tierra Del Fuego, Argentina. *Marine Geology*, *160*(3–4), 301–326. https://doi.org/10.1016/S0025-3227(99)00021-3
Wu, C., Ullah, M. S., Lu, J., & Bhattacharya, J. P. (2016). Formation of point bars through rising and falling flood stages: Evidence from bar morphology, sediment transport and bed shear stress. *Sedimentology*, *63*(6), 1458–1473. https://doi.org/10.1111/sed.12269
Zhao, K., Coco, G., Gong, Z., Darby, S. E., Lanzoni, S., Xu, F., et al. (2022). A Review on Bank Retreat: Mechanisms, Observations, and Modeling. *Reviews of Geophysics*, *60*(2), 1–51. https://doi.org/10.1029/2021rg000761
Zinger, J. A., Rhoads, B. L., & Best, J. L. (2011). Extreme sediment pulses generated by bend cutoffs along a large meandering river. *Nature Geoscience*, *4*(10), 675–678. https://doi.org/10.1038/ngeo1260

Figures and Tables

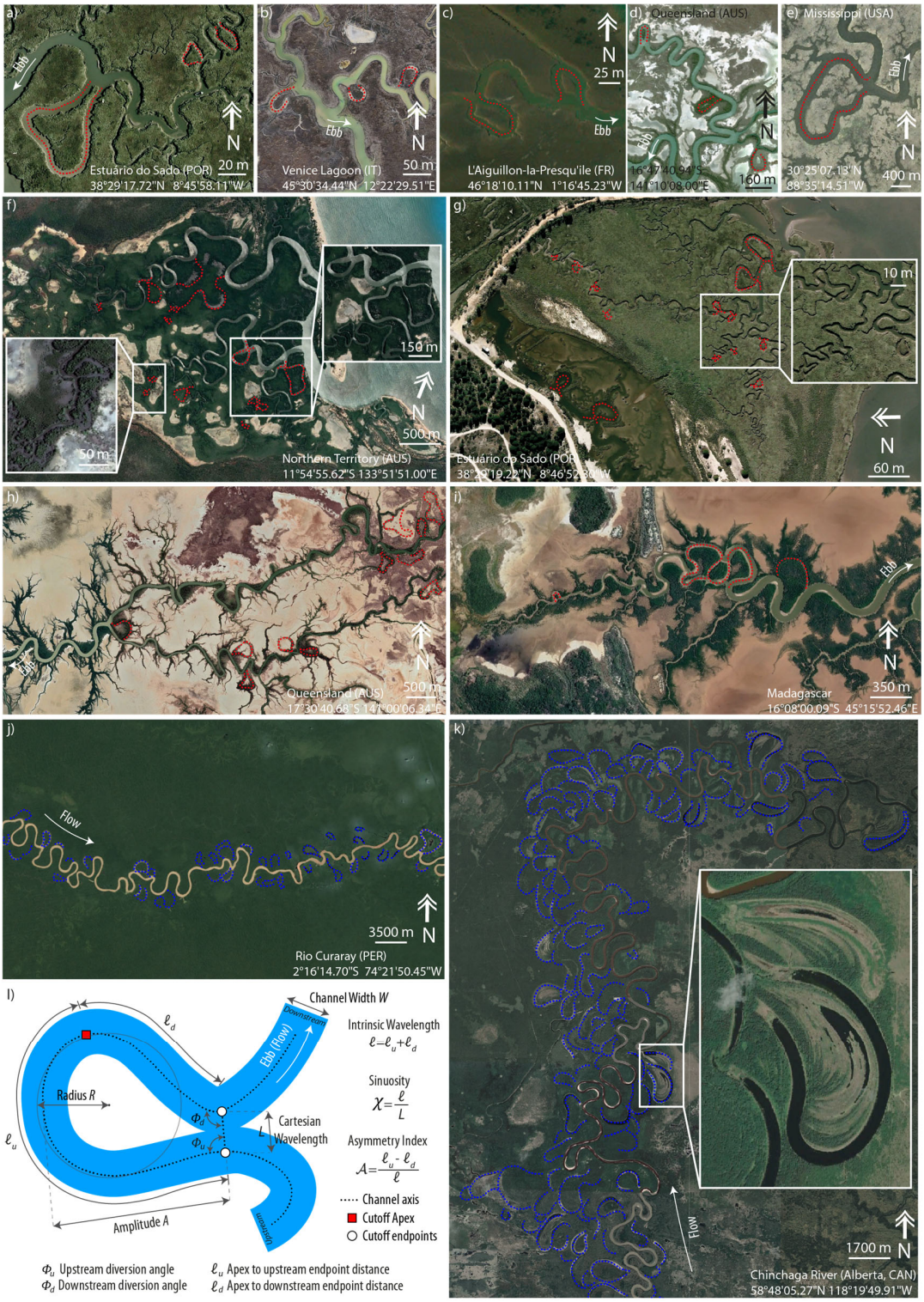

Figure 1. Meander cutoffs in tidal and fluvial landscapes. (a,b,c,d) Examples of individual tidal meander cutoffs from distinct coastal settings worldwide (image© Google, Maxar). (f,g,h,i) Examples of tidal environments characterized by widespread meander cutoffs (image©Google: TerraMetrics, CNES/Airbus,

Maxar, Landsat/Copernicus). (j,k) Examples of river floodplains littered by oxbow lakes and cutoff traces (image©Google: Maxar). Geographic coordinates are reported in each panel. Dotted red and blue lines highlight discernable traces of meander cutoffs in tidal and fluvial landscapes, respectively. l) Sketch illustrating the main morphometric features of meander cutoffs analyzed in this study.

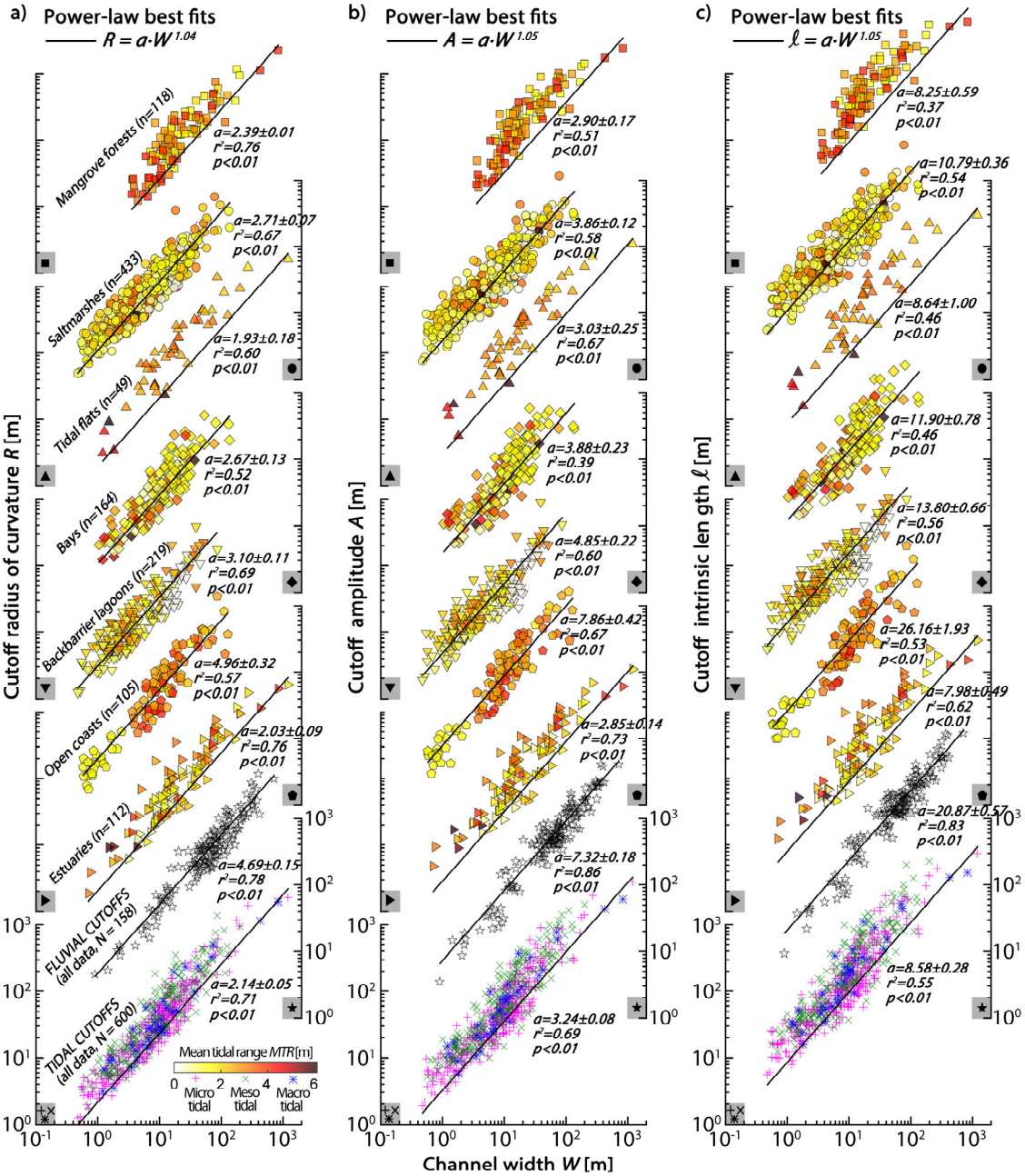

Figure 2. Cutoff morphometrics. Cutoff radius of curvature (R), Amplitude ($\boldsymbol{A}$), and intrinsic length ($\boldsymbol{\ell}$) are plotted against channel width (W) both separately for all tidal and fluvial cutoffs on record and for different tidal-cutoff ensembles based on geomorphological settings and vegetation cover color-coded based on tidal ranges. Continuous black lines represent best-fit power law regressions obtained for different data ensembles, using a common exponent derived from all data and applied to calculate scaling coefficients for each ensemble. Note that the vertical offset among individual data plots is arbitrary: each vertical y-axis ranges from 10^0 to 10^3, and symbols are positioned at the bottom of the axis to aid in identifying the corresponding data plot.

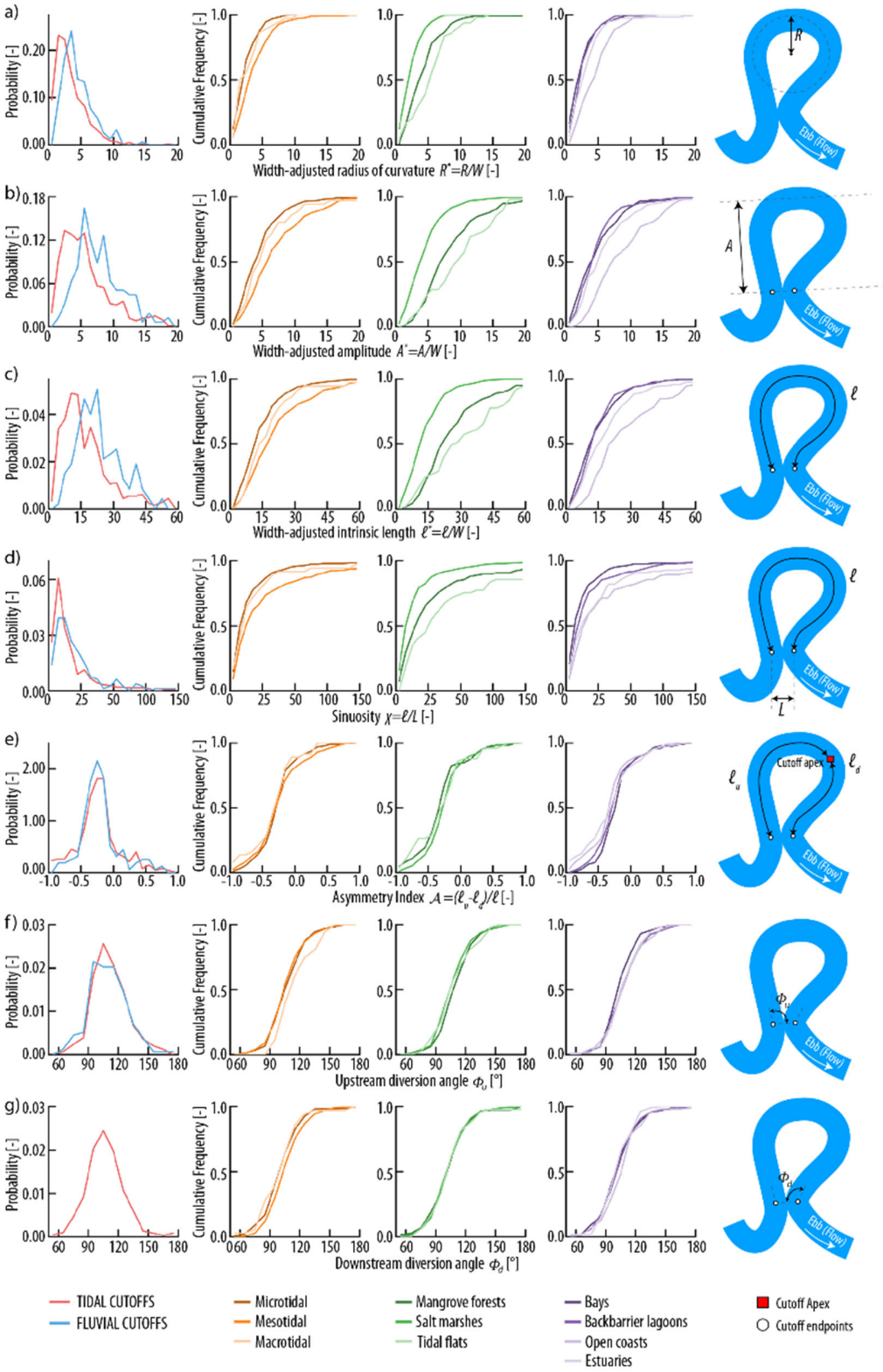

Figure 3. Dimensionless cutoff morphometrics. (a) Width-adjusted radius of curvature; (b) width-adjusted amplitude (c) width-adjusted intrinsic length; (d) sinuosity (χ); (e) asymmetry index ($\mathcal{A}$); (f,g)

upstream and downstream flow-diversion angles ($\boldsymbol{\Phi_u}$ and $\boldsymbol{\Phi_d}$). Panels in the first column show empirical probability distributions for tidal (red) and fluvial (blue) cutoffs. Panels in the other columns report empirical cumulative frequency distributions for tidal cutoffs subdivided based on tidal range, vegetation cover, and geomorphological setting. The fifth column contains sketch-up views for each investigated morphometric.

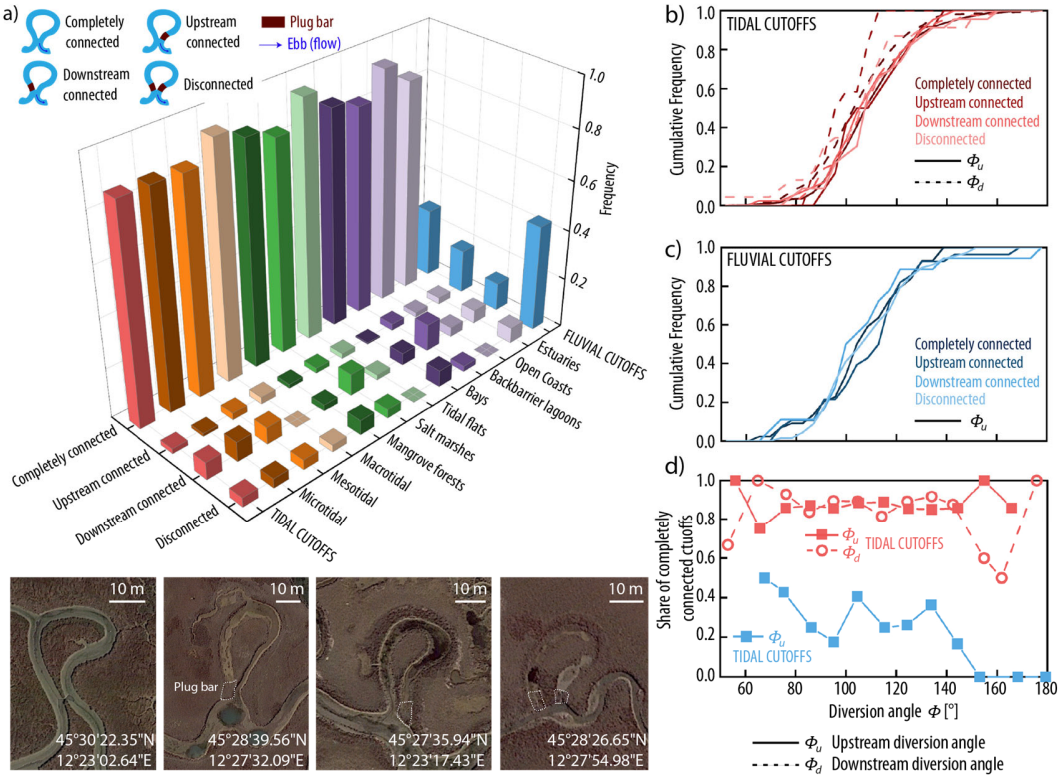

Figure 4. Cutoff connectivity. (a) Barplot showing the relative frequency of different connection types between cutoffs and parent channels, differentiating tidal (red) and fluvial (blue) cutoffs, and further segmenting tidal cutoff ensembles based on tidal range (orange), vegetation cover (green), and geomorphological settings (purple). (b,c) Frequency distributions of flow-diversion angles (Φ) for tidal and fluvial cutoffs. Different colors denote different connectivity with the parent channel. Solid and dashed lines denote upstream and downstream diversion angles, respectively. (d) Share of completely connected tidal (red) and fluvial (blue) cutoffs across uniform 10° diversion-angle intervals. Solid squares and empty dots denote upstream and downstream diversion angles, respectively. (e) Tidal cutoffs found in the microtidal lagoon of Venice (Italy) characterized by different connectivity.

Supporting Information for

Morphometry of tidal meander cutoffs indicates similarity to fluvial morphodynamics

C. Gao[1,2], E. D. Lazarus[3], A. D'Alpaos[2], M. Ghinassi[2], A. Ielpi[4], G. Parker[5,6], A. Rinaldo[7,8], P. Gao[9], Y. P. Wang[1,10], D.Tognin[7], and A. Finotello[2]*

1) Ministry of Education Key Laboratory for Coast and Island Development, School of Geographic and Oceanographic Sciences, Nanjing University, Nanjing, China.
2) Department of Geosciences, University of Padova, Padova, Italy.
3) School of Geography & Environmental Science, University of Southampton, Southampton, UK.
4) Department of Earth, Environmental and Geographic Sciences, University of British Columbia-Okanagan, Kelowna, BC, Canada
5) Department of Civil & Environmental Engineering, University of Illinois, Urbana-Champaign, IL, USA
6) Department of Geology, University of Illinois, Urbana-Champaign, IL, USA
7) Department of Civil, Architectural and Environmental Engineering, University of Padova, Padova, Italy
8) Laboratory of Ecohydrology, École Polytechnique Fédérale de Lausanne, Lausanne, Switzerland
9) Department of Geography and the Environment, Syracuse University, Syracuse, NY, USA
10) State Key Laboratory of Estuarine and Coastal Research, School of Marine Sciences, East China Normal University, Shanghai, China

**Corresponding author: Alvise Finotello (alvise.finotello@unipd.it)*

Contents of this file

Figures S1 to S10
Tables S1 to S13

Figure S1. Examples of tidal cutoffs found in tidal environments characterized by different tidal regimes, vegetation coverages, and geomorphological settings.

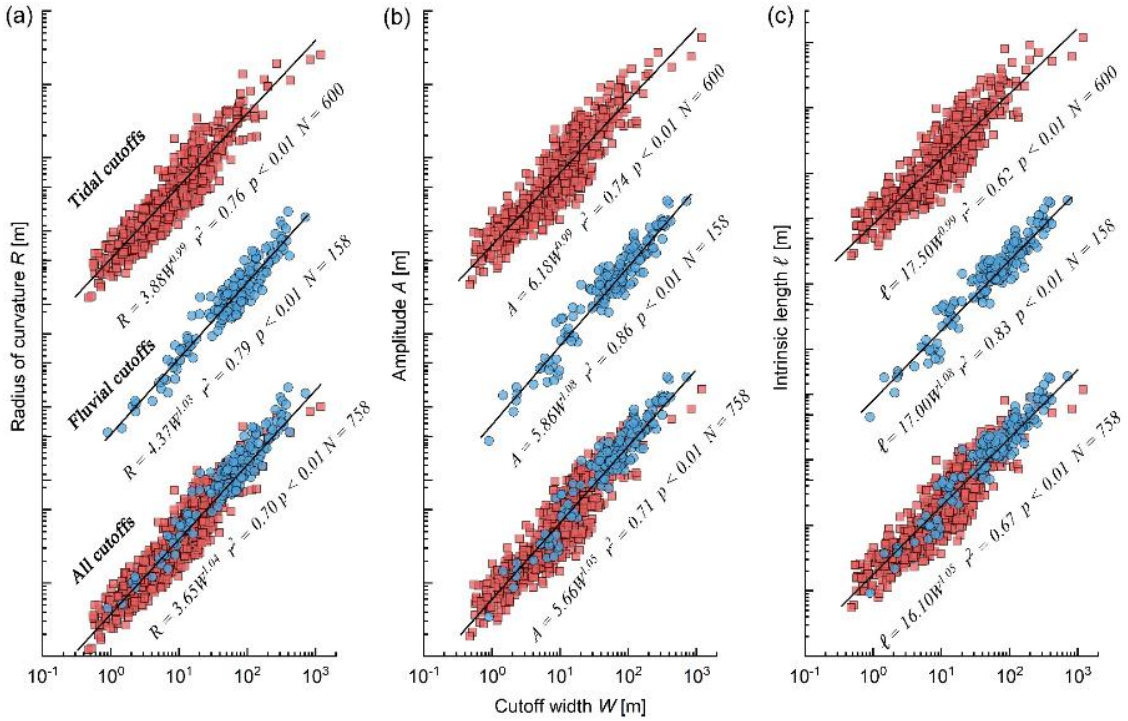

Figure S2. Planform morphometrics of tidal and fluvial meander cutoffs. The cutoff radius of curvature (R), Amplitude (A), and intrinsic length (ℓ) are plotted against channel width (W). Data are plotted both separately and altogether for tidal (red) and fluvial cutoffs (blue). Note that the vertical offset is arbitrary. Continuous black lines represent best-fit power law regressions for each set of data points.

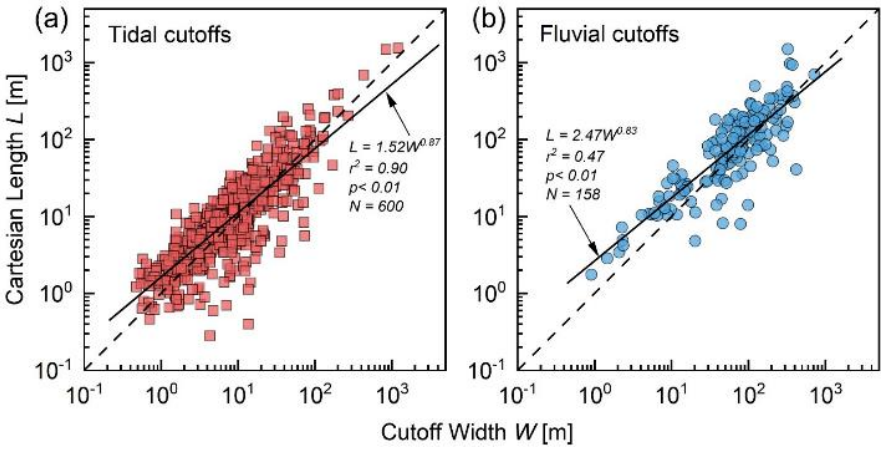

Figure S3. Relationship between cutoff Cartesian length (L) *and channel width* (W) *for (a) tidal and (b) fluvial cutoffs, respectively. The solid lines represent the power-law best fits for all data, whereas dashed lines denote* $L = W$.

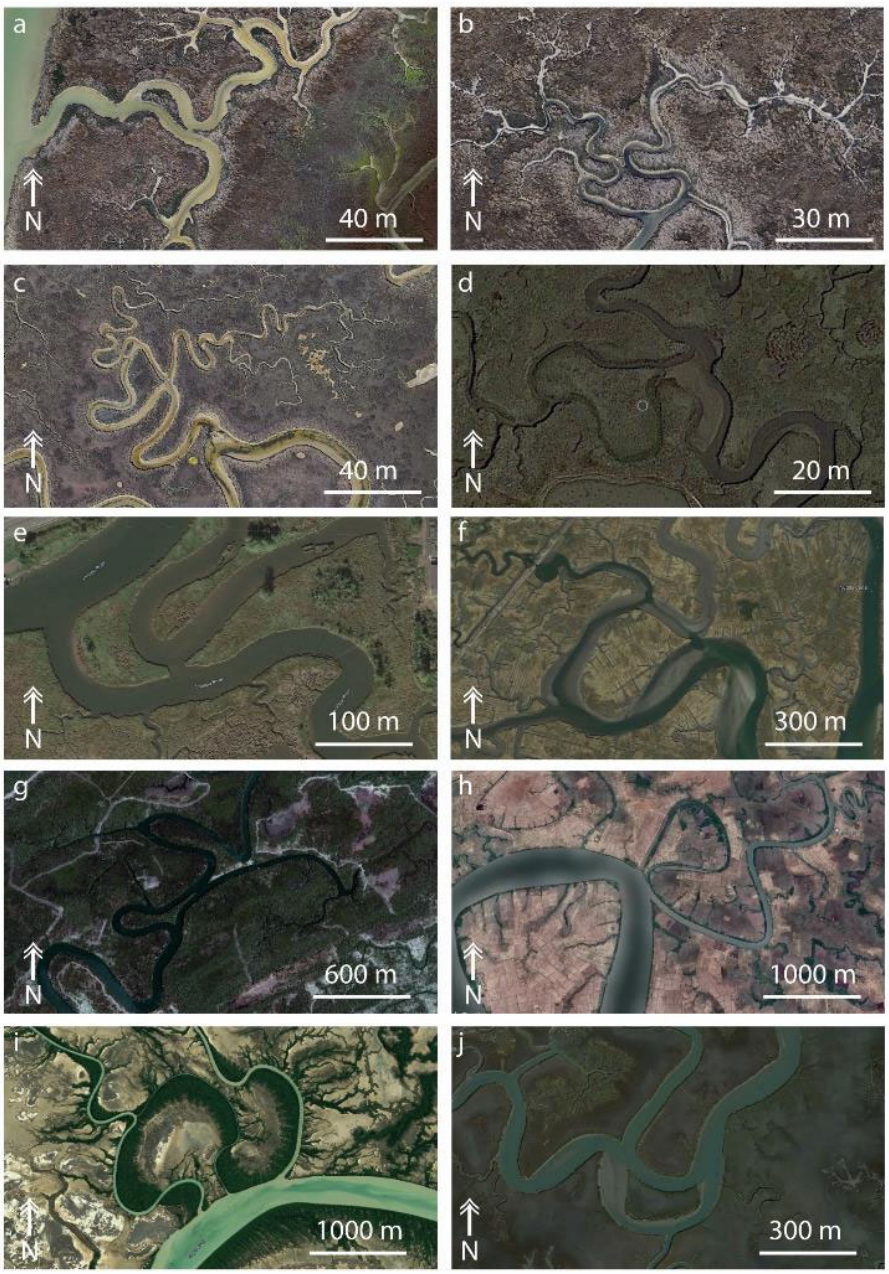

Figure S4. Examples of tidal channel piracies (i.e., captures) from different tidal environments worldwide. a,b,c,) Pagliaga salt marsh, Venice Lagoon, Italy (image ©Google, unknown). d) Ile aux Oiseaux, Aranchon Bay, France (image ©Google, unknown). e) Willapa River, Washington, USA (image ©Google, unknown). f) Hampton, New Hampshire, USA (image ©Google, unknown). g) Pyin Ah Lan/Poe Laung, Myanmar (image ©Google, Maxar technologies). h) Irawaddy River Delta, Myanmar (image ©Google, Maxar technologies). i) Rope River Estuary, Northern Territory, Australia (image ©Google, Maxar technologies). l) Cape Romain National Wildlife Refuge, South Carolina, USA (image ©Google, unknown).

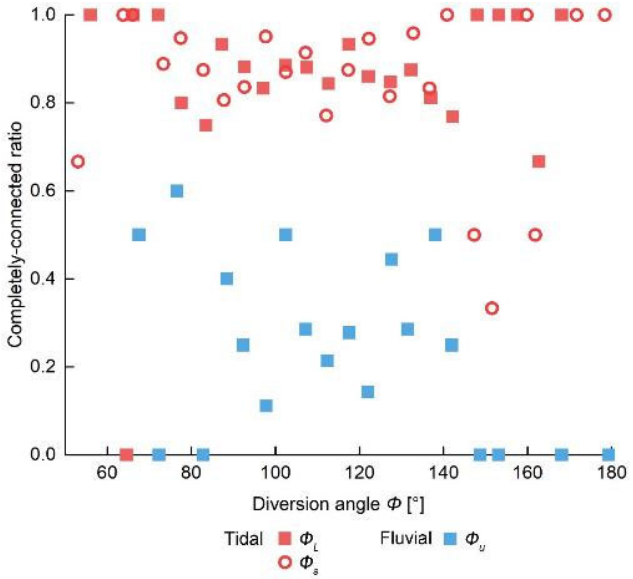

Figure S5. Shares of completely connected cutoffs as a function of diversion angle, computed by binning data based on equally spaced Φ interval (bin size = 5°) and then dividing the number of completely connected cutoffs by the total number of cutoffs in each interval. Tidal and fluvial cutoff data are plotted in red and blue colors, with solid squares and empty dots denoting upstream and downstream diversion angles, respectively.

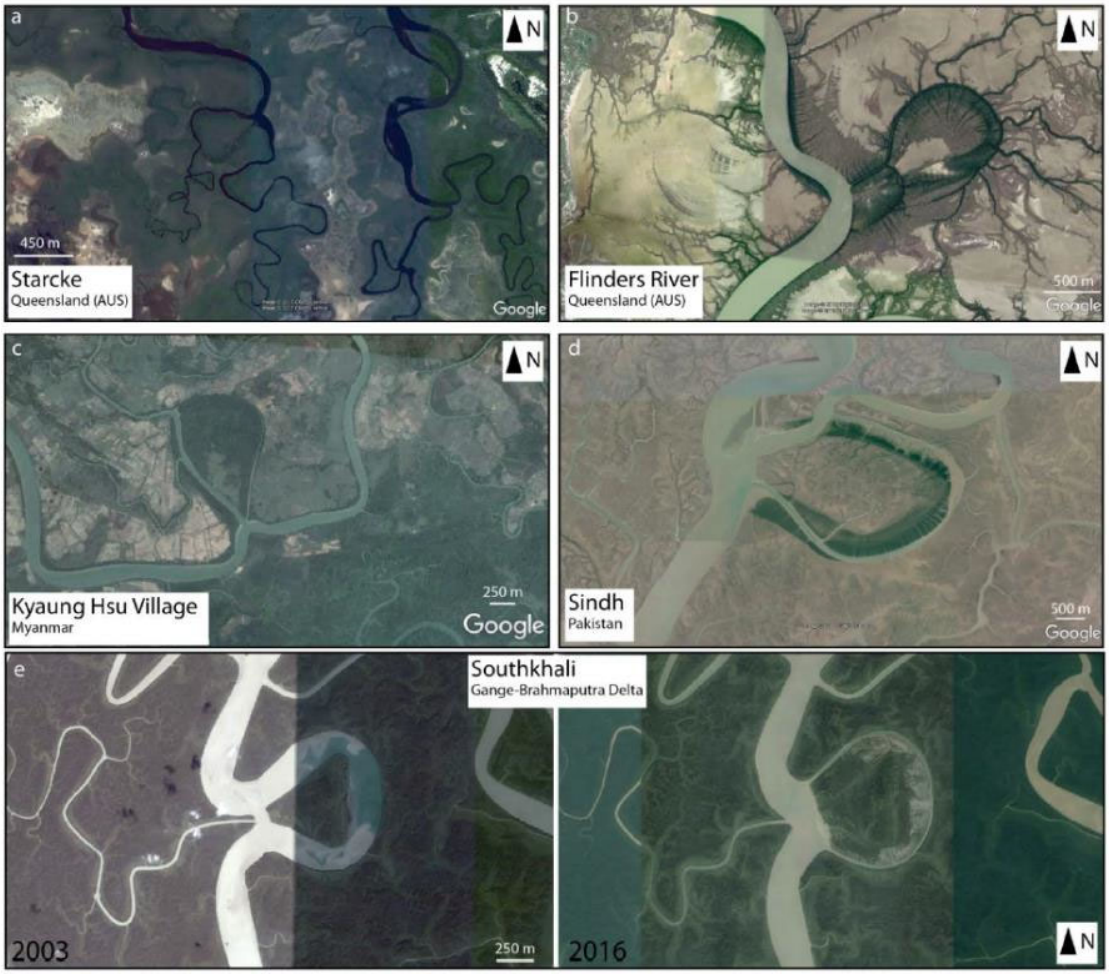

Figure S6. Examples of tidal cutoff remaining either partially or completely connected to their parent channels while keep draining water from the surrounding intertidal areas.

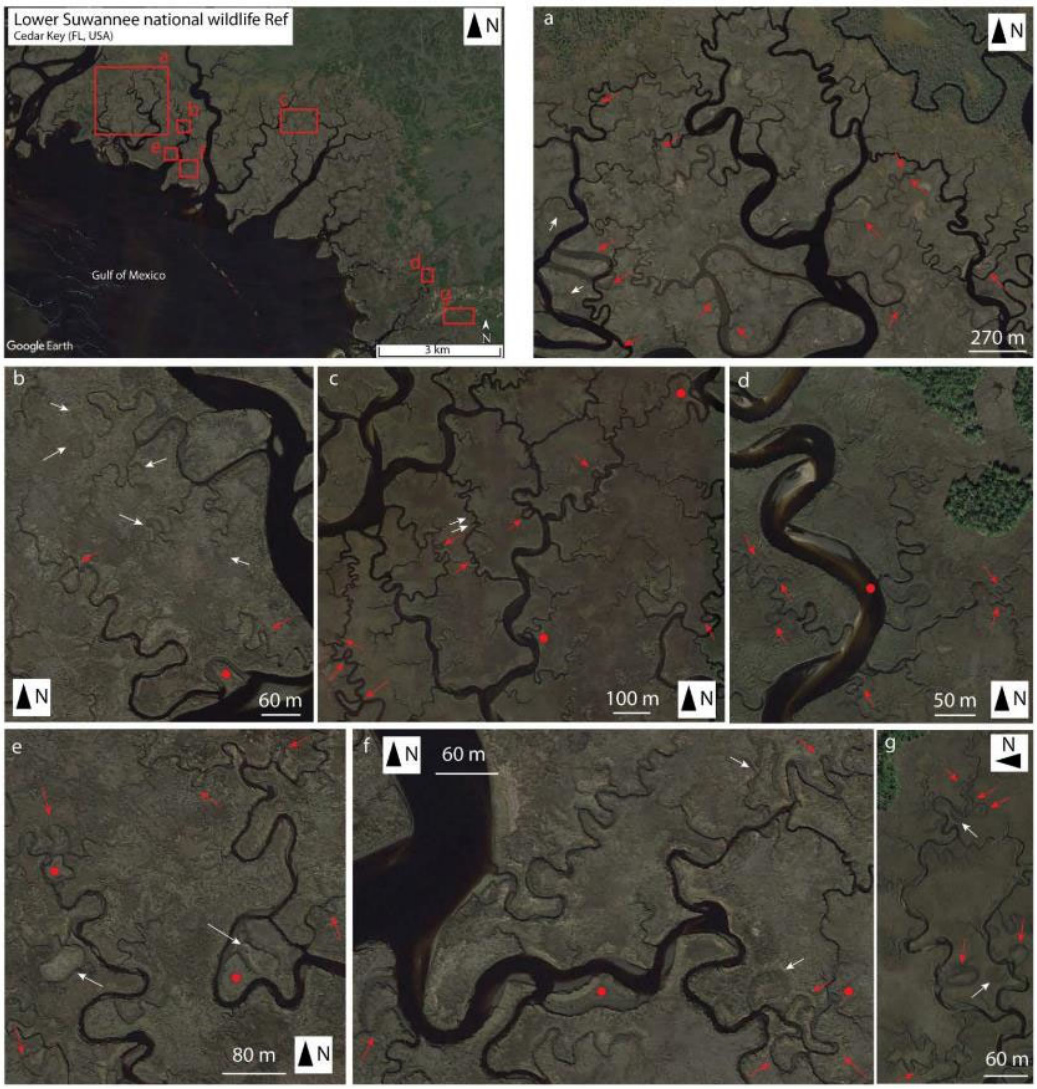

Figure S7. Identification of tidal meander cutoffs within the lower Sawannee National wildlife Ref (FL, USA). Red and white arrows indicate active and relic (i.e., unanalyzed) cutoffs, respectively, whereas red dots identify abandoned channels produced by piracies (i.e., captures) of two adjoining channels.

Figure S8. Identification of tidal meander cutoffs in different tidal settings worldwide. Red and white arrows indicate active and relic (i.e., unanalyzed) cutoffs, respectively.

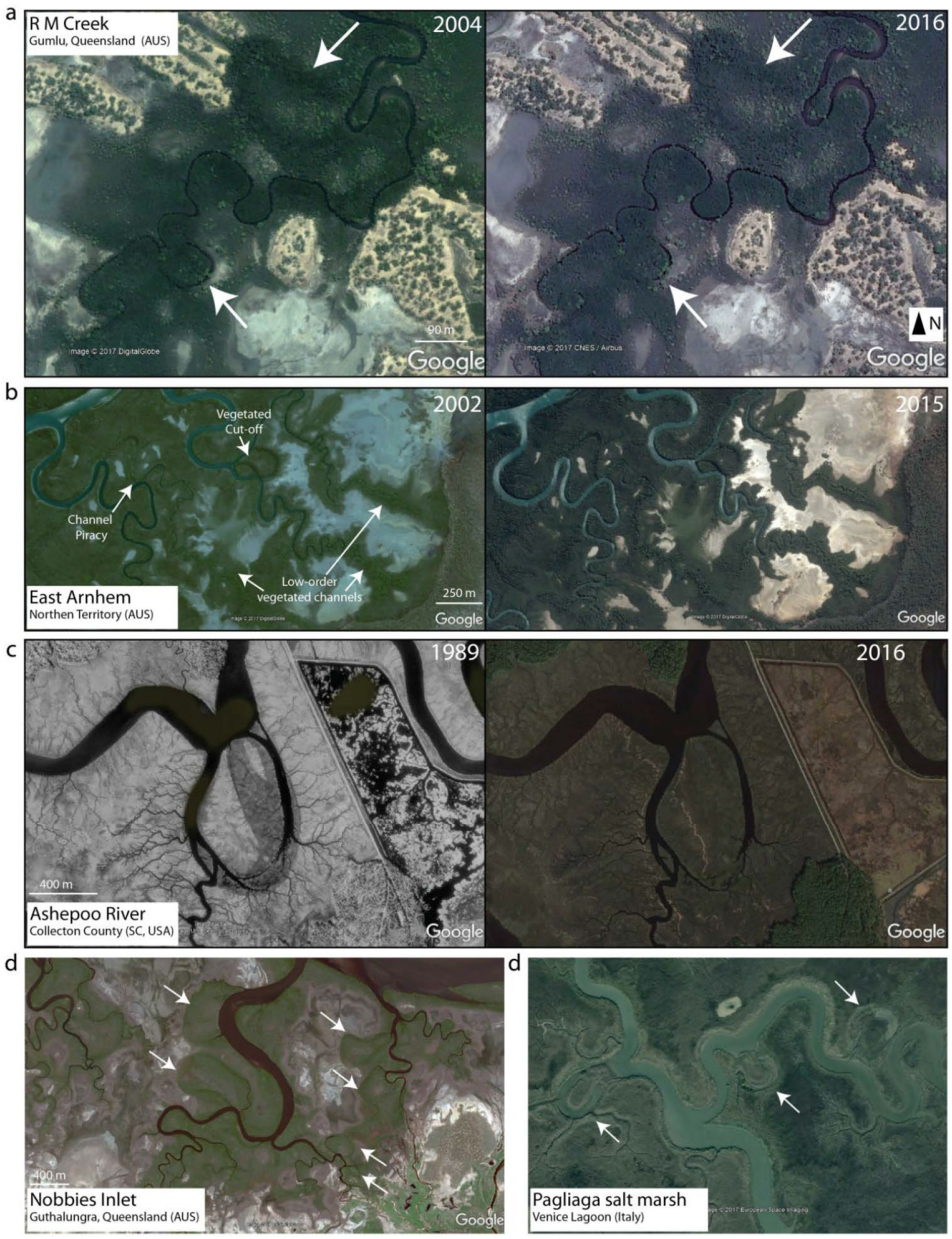

Figure S9. Examples of tidal meander cutoffs colonized by dense halophytic vegetation and/or incorporated into broader drainage network.

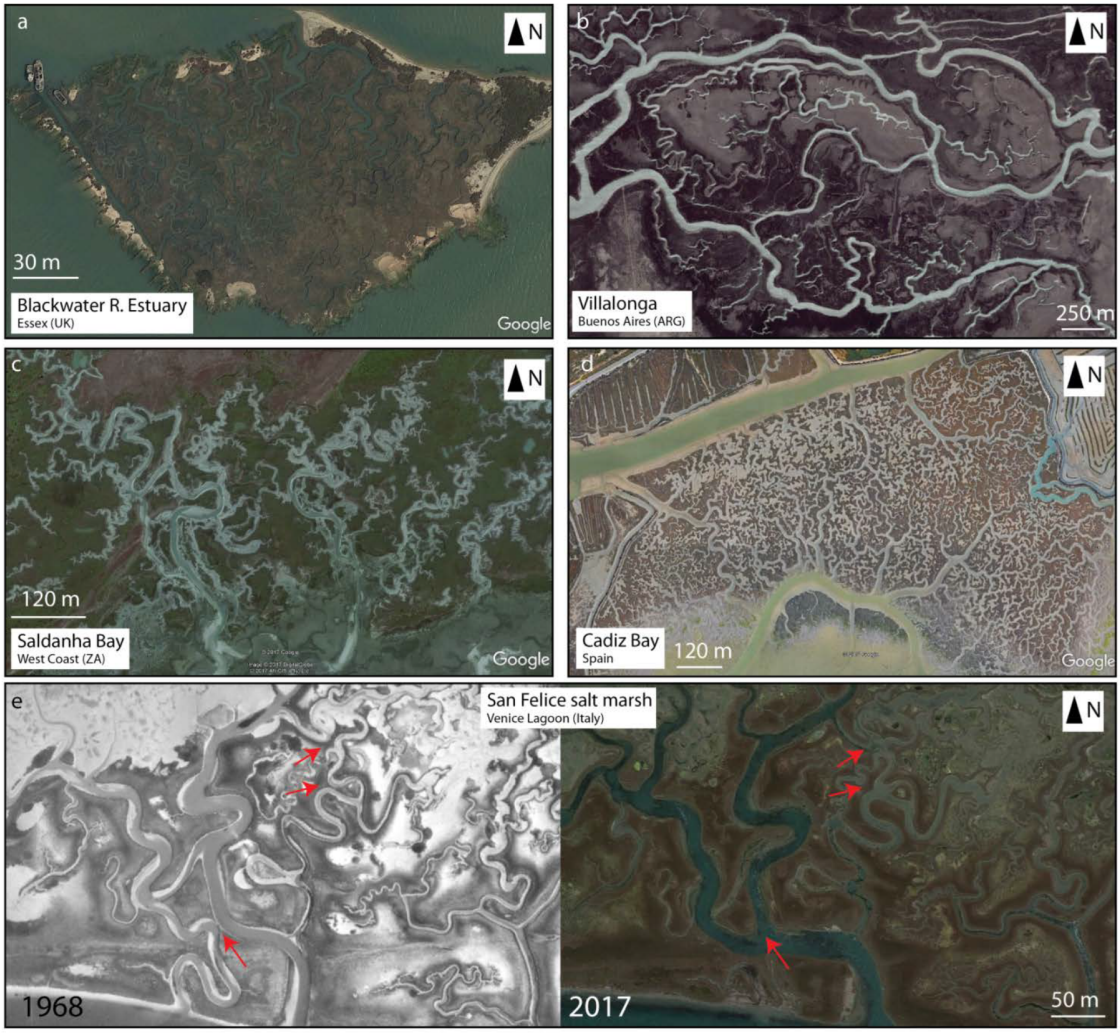

Figure S10. Examples of tidal wetlands characterized by high drainage densities that potentially limit freely meandering of tidal streams, as illustrated by the example reported in the bottom panel.

Table S1. *KS test for tidal cutoffs and fluvial cutoffs (α = 0.05)*

Variable	*Null Hypothesis* H_0	*Alternative Hyp.* H_1	*Rejected Null Hypothesis*	*p-value*
R^*	$cdf_{tidal} = cdf_{fluvial}$	$cdf_{tidal} \neq cdf_{fluvial}$	*Yes*	$4.53e^{-9}$
	$cdf_{tidal} = cdf_{fluvial}$	$cdf_{tidal} > cdf_{fluvial}$	*Yes*	$2.27e^{-9}$
A^*	$cdf_{tidal} = cdf_{fluvial}$	$cdf_{tidal} \neq cdf_{fluvial}$	*Yes*	$3.17e^{-12}$
	$cdf_{tidal} = cdf_{fluvial}$	$cdf_{tidal} > cdf_{fluvial}$	*Yes*	$1.58e^{-12}$
ℓ^*	$cdf_{tidal} = cdf_{fluvial}$	$cdf_{tidal} \neq cdf_{fluvial}$	*Yes*	$8.56e^{-12}$
	$cdf_{tidal} = cdf_{fluvial}$	$cdf_{tidal} > cdf_{fluvial}$	*Yes*	$4.28e^{-12}$
χ	$cdf_{tidal} = cdf_{fluvial}$	$cdf_{tidal} \neq cdf_{fluvial}$	*Yes*	$6.28e^{-4}$
	$cdf_{tidal} = cdf_{fluvial}$	$cdf_{tidal} > cdf_{fluvial}$	*Yes*	$3.14e^{-4}$
$\mathcal{A}$	$cdf_{tidal} = cdf_{fluvial}$	$cdf_{tidal} \neq cdf_{fluvial}$	*No*	$4.90e^{-1}$
Φ_u	$cdf_{tidal} = cdf_{fluvial}$	$cdf_{tidal} \neq cdf_{fluvial}$	*No*	$4.22e^{-1}$

Table S2. *KS test for microtidal cutoffs and mesotidal cutoffs (α = 0.05)*

Variable	*Null Hypothesis* H_0	*Alternative Hyp.* H_1	*Rejected Null Hypothesis*	*p-value*
R^*	$cdf_{micro} = cdf_{meso}$	$cdf_{micro} \neq cdf_{meso}$	*Yes*	$2.49e^{-7}$
	$cdf_{micro} = cdf_{meso}$	$cdf_{micro} > cdf_{meso}$	*Yes*	$1.25e^{-7}$
A^*	$cdf_{micro} = cdf_{meso}$	$cdf_{micro} \neq cdf_{meso}$	*Yes*	$1.42e^{-8}$
	$cdf_{micro} = cdf_{meso}$	$cdf_{micro} > cdf_{meso}$	*Yes*	$7.10e^{-9}$
ℓ^*	$cdf_{micro} = cdf_{meso}$	$cdf_{micro} \neq cdf_{meso}$	*Yes*	$3.62e^{-7}$
	$cdf_{micro} = cdf_{meso}$	$cdf_{micro} > cdf_{meso}$	*Yes*	$1.81e^{-7}$
χ	$cdf_{micro} = cdf_{meso}$	$cdf_{micro} \neq cdf_{meso}$	*Yes*	$1.62e^{-6}$
	$cdf_{micro} = cdf_{meso}$	$cdf_{micro} > cdf_{meso}$	*Yes*	$8.12e^{-7}$
$\mathcal{A}$	$cdf_{micro} = cdf_{meso}$	$cdf_{micro} \neq cdf_{meso}$	*No*	$3.60e^{-1}$
Φ_u	$cdf_{micro} = cdf_{meso}$	$Cdf_{micro} \neq cdf_{meso}$	*No*	$6.80e^{-1}$
Φ_d	$Cdf_{micro} = cdf_{meso}$	$Cdf_{micro} \neq cdf_{meso}$	*No*	$3.00e^{-1}$

Table S3. *KS test for microtidal cutoffs and macrotidal cutoffs (α = 0.05)*

Variable	*Null Hypothesis* H_0	*Alternative Hyp.* H_1	*Rejected Null Hypothesis*	*p-value*
R^*	$cdf_{micro} = cdf_{macro}$	$cdf_{micro} \neq cdf_{macro}$	*No*	$6.30e^{-1}$
A^*	$cdf_{micro} = cdf_{macro}$	$cdf_{micro} \neq cdf_{macro}$	*No*	$5.10e^{-1}$
ℓ^*	$cdf_{micro} = cdf_{macro}$	$cdf_{micro} \neq cdf_{macro}$	*No*	$3.90e^{-1}$
χ	$cdf_{micro} = cdf_{macro}$	$cdf_{micro} \neq cdf_{macro}$	*No*	$7.30e^{-1}$
$\mathcal{A}$	$cdf_{micro} = cdf_{macro}$	$cdf_{micro} \neq cdf_{macro}$	*No*	$8.30e^{-1}$
Φ_u	$cdf_{micro} = cdf_{macro}$	$cdf_{micro} \neq cdf_{macro}$	*No*	$3.00e^{-1}$
Φ_d	$cdf_{micro} = cdf_{macro}$	$cdf_{micro} \neq cdf_{macro}$	*No*	$6.70e^{-1}$

Table S4. *KS test for mesotidal cutoffs and macrotidal cutoffs (α = 0.05)*

Variable	*Null Hypothesis* H_0	*Alternative Hyp.* H_1	*Rejected Null Hypothesis*	*p-value*
R^*	$cdf_{meso} = cdf_{macro}$	$cdf_{meso} \neq cdf_{macro}$	*No*	$1.00e^{-2}$
A^*	$cdf_{meso} = cdf_{macro}$	$cdf_{meso} \neq cdf_{macro}$	*No*	$1.90e^{-1}$
ℓ^*	$cdf_{meso} = cdf_{macro}$	$cdf_{meso} \neq cdf_{macro}$	*No*	$3.70e^{-1}$
χ	$cdf_{meso} = cdf_{macro}$	$cdf_{meso} \neq cdf_{macro}$	*No*	$2.70e^{-1}$
$\mathcal{A}$	$cdf_{meso} = cdf_{macro}$	$cdf_{meso} \neq cdf_{macro}$	*No*	$8.20e^{-1}$
Φ_u	$cdf_{meso} = cdf_{macro}$	$cdf_{meso} \neq cdf_{macro}$	*No*	$5.00e^{-2}$
Φ_d	$cdf_{meso} = cdf_{macro}$	$cdf_{meso} \neq cdf_{macro}$	*No*	$2.70e^{-1}$

Table S5. *KS test for mangrove swamp cutoffs and salt marsh cutoffs (α = 0.05)*

Variable	*Null Hypothesis* H_0	*Alternative Hyp.* H_1	*Rejected Null Hypothesis*	*p-value*
R^*	$cdf_{mangrove} = cdf_{marsh}$	$cdf_{mangrove} \neq cdf_{marsh}$	*Yes*	$3.20e^{-9}$
	$cdf_{mangrove} = cdf_{marsh}$	$cdf_{mangrove} > cdf_{marsh}$	*No*	*1.00*
	$cdf_{mangrove} = cdf_{marsh}$	$cdf_{mangrove} < cdf_{marsh}$	*Yes*	$1.60e^{-9}$
A^*	$cdf_{mangrove} = cdf_{marsh}$	$cdf_{mangrove} \neq cdf_{marsh}$	*Yes*	$2.33e^{-15}$
	$cdf_{mangrove} = cdf_{marsh}$	$cdf_{mangrove} > cdf_{marsh}$	*No*	*1.00*
	$cdf_{mangrove} = cdf_{marsh}$	$cdf_{mangrove} < cdf_{marsh}$	*Yes*	$1.17e^{-15}$
ℓ^*	$cdf_{mangrove} = cdf_{marsh}$	$cdf_{mangrove} \neq cdf_{marsh}$	*Yes*	$9.66e^{-17}$
	$cdf_{mangrove} = cdf_{marsh}$	$cdf_{mangrove} > cdf_{marsh}$	*No*	*1.00*
	$cdf_{mangrove} = cdf_{marsh}$	$cdf_{mangrove} < cdf_{marsh}$	*Yes*	$4.83e^{-17}$
χ	$cdf_{mangrove} = cdf_{marsh}$	$cdf_{mangrove} \neq cdf_{marsh}$	*Yes*	$5.58e^{-6}$
	$cdf_{mangrove} = cdf_{marsh}$	$cdf_{mangrove} > cdf_{marsh}$	*No*	*1.00*
	$cdf_{mangrove} = cdf_{marsh}$	$cdf_{mangrove} < cdf_{marsh}$	*Yes*	$2.79e^{-6}$
$\mathcal{A}$	$cdf_{mangrove} = cdf_{marsh}$	$cdf_{mangrove} \neq cdf_{marsh}$	*No*	$2.00e^{-2}$
Φ_u	$cdf_{mangrove} = cdf_{marsh}$	$cdf_{mangrove} \neq cdf_{marsh}$	*No*	$2.10e^{-1}$
Φ_d	$cdf_{mangrove} = cdf_{marsh}$	$cdf_{mangrove} \neq cdf_{marsh}$	*No*	$6.70e^{-1}$

Table S6. *KS test for mangrove swamp cutoffs and tidal flat cutoffs (α = 0.05)*

Variable	*Null Hypothesis* H_0	*Alternative Hyp.* H_1	*Rejected Null Hypothesis*	*p-value*
R^*	$cdf_{mangrove} = cdf_{flat}$	$cdf_{mangrove} \neq cdf_{flat}$	*Yes*	$7.00e^{-3}$
	$cdf_{mangrove} = cdf_{flat}$	$cdf_{mangrove} > cdf_{flat}$	*Yes*	$3.00e^{-3}$
A^*	$cdf_{mangrove} = cdf_{flat}$	$cdf_{mangrove} \neq cdf_{flat}$	*No*	$3.00e^{-2}$
ℓ^*	$cdf_{mangrove} = cdf_{flat}$	$cdf_{mangrove} \neq cdf_{flat}$	*No*	$4.00e^{-2}$
χ	$cdf_{mangrove} = cdf_{flat}$	$cdf_{mangrove} \neq cdf_{flat}$	*No*	$1.00e^{-1}$
$\mathcal{A}$	$cdf_{mangrove} = cdf_{flat}$	$cdf_{mangrove} \neq cdf_{flat}$	*No*	$2.50e^{-1}$
Φ_u	$cdf_{mangrove} = cdf_{flat}$	$cdf_{mangrove} \neq cdf_{flat}$	*No*	$8.70e^{-1}$
Φ_d	$cdf_{mangrove} = cdf_{flat}$	$cdf_{mangrove} \neq cdf_{flat}$	*No*	$9.90e^{-1}$

Table S7. *KS test for salt marsh cutoffs and tidal flat cutoffs (α = 0.05)*

Variable	Null Hypothesis H_0	Alternative Hyp. H_1	Rejected Null Hypothesis	p-value
R^*	$cdf_{marsh} = cdf_{flat}$	$cdf_{marsh} \neq cdf_{flat}$	Yes	$1.84e^{-11}$
	$cdf_{marsh} = cdf_{flat}$	$cdf_{marsh} > cdf_{flat}$	Yes	$9.20e^{-12}$
A^*	$cdf_{marsh} = cdf_{flat}$	$cdf_{marsh} \neq cdf_{flat}$	Yes	$6.05e^{-13}$
	$cdf_{marsh} = cdf_{flat}$	$cdf_{marsh} > cdf_{flat}$	Yes	$3.02e^{-13}$
ℓ^*	$cdf_{marsh} = cdf_{flat}$	$cdf_{marsh} \neq cdf_{flat}$	Yes	$2.77e^{-12}$
	$cdf_{marsh} = cdf_{flat}$	$cdf_{marsh} > cdf_{flat}$	Yes	$1.38e^{-12}$
χ	$cdf_{marsh} = cdf_{flat}$	$cdf_{marsh} \neq cdf_{flat}$	Yes	$2.69e^{-6}$
	$cdf_{marsh} = cdf_{flat}$	$cdf_{marsh} > cdf_{flat}$	Yes	$1.34e^{-6}$
$\mathcal{A}$	$cdf_{marsh} = cdf_{flat}$	$cdf_{marsh} \neq cdf_{flat}$	No	$6.00e^{-2}$
Φ_u	$cdf_{marsh} = cdf_{flat}$	$cdf_{marsh} \neq cdf_{flat}$	No	$7.00e^{-1}$
Φ_d	$cdf_{marsh} = cdf_{flat}$	$cdf_{marsh} \neq cdf_{flat}$	No	1.00

Table S8. *KS test for bay cutoffs and lagoon cutoffs (α = 0.05)*

Variable	Null Hypothesis H_0	Alternative Hyp. H_1	Rejected Null Hypothesis	p-value
R^*	$cdf_{bay} = cdf_{lagoon}$	$cdf_{bay} \neq cdf_{lagoon}$	No	$2.62e^{-1}$
A^*	$cdf_{bay} = cdf_{lagoon}$	$cdf_{bay} \neq cdf_{lagoon}$	No	$1.50e^{-1}$
ℓ^*	$cdf_{bay} = cdf_{lagoon}$	$cdf_{bay} \neq cdf_{lagoon}$	No	$1.58e^{-1}$
χ	$cdf_{bay} = cdf_{lagoon}$	$cdf_{bay} \neq cdf_{lagoon}$	No	$5.67e^{-2}$
$\mathcal{A}$	$cdf_{bay} = cdf_{lagoon}$	$cdf_{bay} \neq cdf_{lagoon}$	No	$1.28e^{-1}$
Φ_u	$cdf_{bay} = cdf_{lagoon}$	$cdf_{bay} \neq cdf_{lagoon}$	Yes	$3.09e^{-2}$
	$cdf_{bay} = cdf_{lagoon}$	$cdf_{bay} > cdf_{lagoon}$	Yes	$1.55e^{-2}$
Φ_d	$cdf_{bay} = cdf_{lagoon}$	$cdf_{bay} \neq cdf_{lagoon}$	No	$8.75e^{-1}$

Table S9. *KS test for bay cutoffs and coast cutoffs (α = 0.05)*

Variable	Null Hypothesis H_0	Alternative Hyp. H_1	Rejected Null Hypothesis	p-value
R^*	$cdf_{bay} = cdf_{coast}$	$cdf_{bay} \neq cdf_{coast}$	Yes	$2.04e^{-8}$
	$cdf_{bay} = cdf_{coast}$	$cdf_{bay} > cdf_{coast}$	Yes	$1.02e^{-8}$
A^*	$cdf_{bay} = cdf_{coast}$	$cdf_{bay} \neq cdf_{coast}$	Yes	$3.93e^{-9}$
	$cdf_{bay} = cdf_{coast}$	$cdf_{bay} > cdf_{coast}$	Yes	$1.97e^{-9}$
ℓ^*	$cdf_{bay} = cdf_{coast}$	$cdf_{bay} \neq cdf_{coast}$	Yes	$7.95e^{-10}$
	$cdf_{bay} = cdf_{coast}$	$cdf_{bay} > cdf_{coast}$	Yes	$3.98e^{-10}$
χ	$cdf_{bay} = cdf_{coast}$	$cdf_{bay} \neq cdf_{coast}$	Yes	$2.16e^{-5}$
	$cdf_{bay} = cdf_{coast}$	$cdf_{bay} > cdf_{coast}$	Yes	$1.08e^{-5}$
$\mathcal{A}$	$cdf_{bay} = cdf_{coast}$	$cdf_{bay} \neq cdf_{coast}$	Yes	$1.2e^{-3}$
	$cdf_{bay} = cdf_{coast}$	$cdf_{bay} > cdf_{coast}$	No	$9.84e^{-1}$
	$cdf_{bay} = cdf_{coast}$	$cdf_{bay} < cdf_{coast}$	Yes	$5.85e^{-4}$
Φ_u	$cdf_{bay} = cdf_{coast}$	$cdf_{bay} \neq cdf_{coast}$	No	$9.89e^{-2}$
Φ_d	$cdf_{bay} = cdf_{coast}$	$cdf_{bay} \neq cdf_{coast}$	Yes	$3.05e^{-2}$
	$cdf_{bay} = cdf_{coast}$	$cdf_{bay} > cdf_{coast}$	Yes	$1.53e^{-2}$

Table S10. *KS test for bay cutoffs and estuary cutoffs (α = 0.05)*

Variable	Null Hypothesis H_0	Alternative Hyp. H_1	Rejected Null Hypothesis	p-value
R^*	$cdf_{bay} = cdf_{estuary}$	$cdf_{bay} \neq cdf_{estuary}$	Yes	$1.70e^{-2}$
	$cdf_{bay} = cdf_{estuary}$	$cdf_{bay} > cdf_{estuary}$	Yes	$8.5e^{-3}$
A^*	$cdf_{bay} = cdf_{estuary}$	$cdf_{bay} \neq cdf_{estuary}$	Yes	$3.71e^{-2}$
	$cdf_{bay} = cdf_{estuary}$	$cdf_{bay} > cdf_{estuary}$	Yes	$1.85e^{-2}$
ℓ^*	$cdf_{bay} = cdf_{estuary}$	$cdf_{bay} \neq cdf_{estuary}$	No	$6.37e^{-2}$
χ	$cdf_{bay} = cdf_{estuary}$	$cdf_{bay} \neq cdf_{estuary}$	Yes	$6.39e^{-4}$
	$cdf_{bay} = cdf_{estuary}$	$cdf_{bay} > cdf_{estuary}$	Yes	$3.20e^{-4}$
$\mathcal{A}$	$cdf_{bay} = cdf_{estuary}$	$cdf_{bay} \neq cdf_{estuary}$	Yes	$1.50e^{-3}$
	$cdf_{bay} = cdf_{estuary}$	$cdf_{bay} > cdf_{estuary}$	No	$8.21e^{-1}$
	$cdf_{bay} = cdf_{estuary}$	$cdf_{bay} < cdf_{estuary}$	Yes	$7.55e^{-4}$
Φ_u	$cdf_{bay} = cdf_{estuary}$	$cdf_{bay} \neq cdf_{estuary}$	No	$7.27e^{-2}$
Φ_d	$cdf_{bay} = cdf_{estuary}$	$cdf_{bay} \neq cdf_{estuary}$	No	$5.74e^{-1}$

Table S11. *KS test for lagoon cutoffs and coast cutoffs (α = 0.05)*

Variable	Null Hypothesis H_0	Alternative Hyp. H_1	Rejected Null Hypothesis	p-value
R^*	$cdf_{lagoon} = cdf_{coast}$	$cdf_{lagoon} \neq cdf_{coast}$	Yes	$6.08e^{-8}$
	$cdf_{lagoon} = cdf_{coast}$	$cdf_{lagoon} > cdf_{coast}$	Yes	$3.04e^{-8}$
A^*	$cdf_{lagoon} = cdf_{coast}$	$cdf_{lagoon} \neq cdf_{coast}$	Yes	$4.95e^{-11}$
	$cdf_{lagoon} = cdf_{coast}$	$cdf_{lagoon} > cdf_{coast}$	Yes	$2.47e^{-11}$
ℓ^*	$cdf_{lagoon} = cdf_{coast}$	$cdf_{lagoon} \neq cdf_{coast}$	Yes	$5.48e^{-12}$
	$cdf_{lagoon} = cdf_{coast}$	$cdf_{lagoon} > cdf_{coast}$	Yes	$2.74e^{-12}$
χ	$cdf_{lagoon} = cdf_{coast}$	$cdf_{lagoon} \neq cdf_{coast}$	Yes	$1.39e^{-2}$
	$cdf_{lagoon} = cdf_{coast}$	$cdf_{lagoon} > cdf_{coast}$	Yes	$6.90e^{-3}$
$\mathcal{A}$	$cdf_{lagoon} = cdf_{coast}$	$cdf_{lagoon} \neq cdf_{coast}$	No	$5.76e^{-2}$
Φ_u	$cdf_{lagoon} = cdf_{coast}$	$cdf_{lagoon} \neq cdf_{coast}$	No	$9.83e^{-1}$
Φ_d	$cdf_{lagoon} = cdf_{coast}$	$cdf_{lagoon} \neq cdf_{coast}$	No	$1.83e^{-1}$

Table S12. *KS test for lagoon cutoffs and estuary cutoffs (α = 0.05)*

Variable	Null Hypothesis H_0	Alternative Hyp. H_1	Rejected Null Hypothesis	p-value
R^*	$cdf_{lagoon} = cdf_{estuary}$	$cdf_{lagoon} \neq cdf_{estuary}$	No	$5.65e^{-2}$
A^*	$cdf_{lagoon} = cdf_{estuary}$	$cdf_{lagoon} \neq cdf_{estuary}$	Yes	$4.9e^{-3}$
	$cdf_{lagoon} = cdf_{estuary}$	$cdf_{lagoon} > cdf_{estuary}$	Yes	$2.5e^{-3}$
ℓ^*	$cdf_{lagoon} = cdf_{estuary}$	$cdf_{lagoon} \neq cdf_{estuary}$	Yes	$2.17e^{-2}$
	$cdf_{lagoon} = cdf_{estuary}$	$cdf_{lagoon} > cdf_{estuary}$	Yes	$1.09e^{-2}$
χ	$cdf_{lagoon} = cdf_{estuary}$	$cdf_{lagoon} \neq cdf_{estuary}$	Yes	$1.58e^{-2}$
	$cdf_{lagoon} = cdf_{estuary}$	$cdf_{lagoon} > cdf_{estuary}$	Yes	$7.9e^{-3}$
$\mathcal{A}$	$cdf_{lagoon} = cdf_{estuary}$	$cdf_{lagoon} \neq cdf_{estuary}$	No	$6.06e^{-2}$
Φ_u	$cdf_{lagoon} = cdf_{estuary}$	$cdf_{lagoon} \neq cdf_{estuary}$	No	$7.48e^{-1}$
Φ_d	$cdf_{lagoon} = cdf_{estuary}$	$cdf_{lagoon} \neq cdf_{estuary}$	No	$5.96e^{-1}$

Table S13. *KS test for coast cutoffs and estuary cutoffs (α = 0.05)*

Variable	*Null Hypothesis* H_0	*Alternative Hyp.* H_1	*Rejected Null Hypothesis*	*p-value*
R^*	$cdf_{coast} = cdf_{estuary}$	$cdf_{coast} \neq cdf_{estuary}$	*Yes*	$9.88e^{-5}$
	$cdf_{coast} = cdf_{estuary}$	$cdf_{coast} > cdf_{estuary}$	*No*	$9.65e^{-1}$
	$cdf_{coast} = cdf_{estuary}$	$cdf_{coast} < cdf_{estuary}$	*Yes*	$4.94e^{-5}$
A^*	$cdf_{coast} = cdf_{estuary}$	$cdf_{coast} \neq cdf_{estuary}$	*Yes*	$8.66e^{-4}$
	$cdf_{coast} = cdf_{estuary}$	$cdf_{coast} > cdf_{estuary}$	*No*	$9.65e^{-1}$
	$cdf_{coast} = cdf_{estuary}$	$cdf_{coast} < cdf_{estuary}$	*Yes*	$4.33e^{-4}$
ℓ^*	$cdf_{coast} = cdf_{estuary}$	$cdf_{coast} \neq cdf_{estuary}$	*Yes*	$3.26e^{-4}$
	$cdf_{coast} = cdf_{estuary}$	$cdf_{coast} > cdf_{estuary}$	*No*	$9.91e^{-1}$
	$cdf_{coast} = cdf_{estuary}$	$cdf_{coast} < cdf_{estuary}$	*Yes*	$1.63e^{-4}$
χ	$cdf_{coast} = cdf_{estuary}$	$cdf_{coast} \neq cdf_{estuary}$	*No*	$1.00e^{-1}$
$\mathcal{A}$	$cdf_{coast} = cdf_{estuary}$	$cdf_{coast} \neq cdf_{estuary}$	*No*	$2.43e^{-1}$
Φ_u	$cdf_{coast} = cdf_{estuary}$	$cdf_{coast} \neq cdf_{estuary}$	*No*	$7.76e^{-1}$
Φ_d	$cdf_{coast} = cdf_{estuary}$	$cdf_{coast} \neq cdf_{estuary}$	*Yes*	$3.39e^{-2}$
	$cdf_{coast} = cdf_{estuary}$	$cdf_{coast} > cdf_{estuary}$	*No*	$6.82e^{-1}$
	$cdf_{coast} = cdf_{estuary}$	$cdf_{coast} < cdf_{estuary}$	*Yes*	$1.69e^{-2}$